

Photocages as a New Approach to Modulate Zinc Signals

by

Xiaomeng Liang

A Thesis

Submitted to the Faculty

of the

WORCESTER POLYTECHNIC INSTITUTE

in partial fulfillment of the requirements for the

Degree of Master of Science

in

Chemistry

Aug 2016

Approved by:

Abstract

Zinc is one of the most important trace elements in biological systems. Recent advances confirmed the existence of free (labile) zinc and its dynamic role in cellular responses. Zinc has been increasingly recognized as a signaling molecule. Zinc signaling is caused by alternation in free zinc concentrations. In neurons, zinc is released in synaptic clefts. It mediates cell-to-cell signaling and acts like a neurotransmitter. Zinc is also found to be a second messenger akin to calcium, capable of transducing extracellular stimuli into intracellular signaling events.

The development of photocaged zinc complexes is a very important approach to facilitate zinc homeostasis and signaling study. Taken advantage of light, such tools can provide time and spatial control of zinc release. In the previous study we have reported ZinCasts, ZinCleavs and NTAdCage. Based on these work, here three more photocages are developed and named as DPAdCage, DAPdeCage and XDAPdeCage. These cages adopt a new carbanion-mediated photodecarboxylation strategy and exhibits a prominent improvement in terms of fast photolysis kinetics and biocompatibility. Moreover, both Zn(DAPdeCage) and Zn(XDAPdeCage) are neutral charged complexes therefore can be delivered in cells without extra modification. This is the first time a caged metal complex is reported to be readily cell membrane permeable. While no zinc photocages have been reported in the neurological studies by far, we expect application of these cages in vivo will provide a new technique for those biologists and physiologists who interest in biological free zinc.

Acknowledgement

I would like first to thank my advisor, Prof. Shawn Burdette, for his guidance, assistance and inspiration on my research project. I appreciate his vast knowledge and skill in many areas which gave me a good opportunity to learn chemistry beyond text books and published papers.

Next I would like to thank my committee members for their time and advices on the thesis.

I would also like to thank my lab mates for sharing their knowledge and skills.

A special thank to my friends who always stand by when I need a help or advice on my research. From them I learned a lot of experimental techniques and ideas, such as using own-made TLC plates to purification compounds instead of running long columns. These tricks makes the research work more interesting.

In the end I would like to thank the department for helping me to make my graduate studies.

Contents

Abstract	i
Acknowledgements	ii
List of Figures	v
List of Schemes	vii
I. Introduction: Zinc Homeostasis and Signaling	1
1.1 Zinc in Biological Systems	1
1.2 Zinc Signaling	2
2 Introduction: Photocages	5
2.1 Illuminating Cell Chemistry with a Light Switch.....	5
2.2 Photocaged Metal Ion	6
2.3 Previous Work on Zn ²⁺ Photocages.....	7
3 DPAdCage	10
3.1 Background.....	10
3.2 Experimental Section.....	11
3.2.1 Materials and Methods	11
3.2.2 Synthetic Procedures	12
3.2.3 Determination of Zn ²⁺ Binding Affinity.....	14
3.2.4 Determination of Quantum Efficiency	15
3.2.5 Release of Caged Zn ²⁺	16
3.2.6 Metal Selectivity.....	16
3.3 Results and Discussion	17
3.3.1 Design and Synthesis.....	17
3.3.2 Zn ²⁺ Binding Studies	17
3.3.3 Photochemistry	20
4 DAPdeCage	26
4.1 Background.....	26
4.2 Experimental Section.....	27
4.2.1 Materials and Methods	27
4.2.2 Synthetic Procedures	27

4.2.3 Determination of Zn ²⁺ Binding Constants	30
4.2.4 Quantum Efficiency	31
4.2.5 Release of Caged Zn ²⁺	31
4.2.6 Metal Selectivity.....	32
4.3 Results and Discussion.....	32
4.3.1 Design and Synthesis.....	32
4.3.2 Zn ²⁺ Binding Studies.....	33
4.3.3 Photochemistry.....	36
5 XDAPdeCage	40
5.1 Background.....	40
5.2 Experimental Section.....	40
5.2.1 Materials and Methods	40
5.2.2 Synthetic Procedure.....	40
5.2.3 Determination of Zn ²⁺ Binding Constants.....	43
5.2.4 Quantum Yield of Photolysis	44
5.2.5 Release of Caged Zn ²⁺	45
5.3 Results and Discussion.....	45
5.3.1 Design and Synthesis.....	45
5.3.2 Zn ²⁺ Binding Studies	46
5.3.3 Photochemistry.....	48
6 Summary and Conclusion.....	55
References	58

List of Figures

Fig 1.1 Extracellular zinc signaling.....	2
Fig 1.2 Intracellular zinc signaling	3
Fig 2.1 Examples of photocages for metal ions.....	6
Fig 2.2 Examples of uncaging Zn^{2+} from its photocages.	8
Fig 3.1 Structures of NTA, PDA, BPG and NTAdCage, DPAdCage.	11
Fig 3.2 Competitive titration between DPAdCage and PAR in the presence of Zn^{2+}	18
Fig 3.3 Ca-Zn exchange and Cu-Zn exchange.	20
Fig 3.4 LC traces of DPAdCage before and after irradiation	21
Fig 3.5 LC traces of $[Zn(DPAdCage)]^+$ before and after irradiation	22
Fig 3.6 Fluorescence response of ZTRS upon uncaging of DPAdCage.....	24
Fig 3.7 Zn^{2+} uncaging tracked by the formation of Zn-PAR complex.....	25
Fig 4.1 Zn^{2+} complexes with different charges.	27
Fig 4.2 Competitive titration between DAPdeCage and PAR in the presence of Zn^{2+}	34
Fig 4.3. Ca-Zn exchange evidenced by PAR_2Zn formation..	35
Fig 4.4 LC traces of DAPdeCage before and after irradiation	36
Fig 4.5 LC traces of $Zn(DAPdeCage)$ before and after irradiation	37
Fig 4.6 The Zn^{2+} released from $Zn(DAPdeCage)$ monitored by ZTRS.....	38
Fig 4.7 The Zn^{2+} released from $Zn(DAPdeCage)$ monitored by the formation of PAR_2Zn	39
Fig 5.1 Competitive titration between PAR_2Zn and XDAPdeCage.....	47
Fig 5.2 Ca-Zn exchange evidenced by PAR_2Zn formation.	48
Fig 5.3 Absorbance changes of XDAPdeCage upon irradiation.	50
Fig 5.4 LC traces of XDAPdeCage (H_2O with with 50% CH_3OH as cosolvent) upon photolysis.....	51
Fig 5.5 LC traces of $Zn(XDAPdeCage)$ (H_2O with with 50% CH_3OH as cosolvent) upon photolysis.....	51
Fig 5.6 Proposed photoproducts upon XDAPdeCage uncaging, evidenced from LC-MS.	52
Fig 5.7 LC traces of XDAPdeCage (HEPES with with 50% CH_3OH as cosolvent) before and after photolysis.	52

Fig 5.8 LC traces of Zn(XDAPdeCage) (HEPES with with 50% CH₃OH as cosolvent) before and after photolysis.53

Fig 5.9 Uncaging Zn²⁺ from Zn(XDAPdeCage) monitored by fluorescent sensor ZTRS.54

Fig 6.1 Structures of Zn²⁺ chelators and the corresponding Zn²⁺ cages developed.56

List of Schemes

Scheme 2.1 Photolysis of <i>o</i> -NB caged ATP.....	5
Scheme 3.1 Reaction mechanism of <i>o</i> -nitrobenzyl based photolysis.	10
Scheme 3.2 Photodecarboxylation of NPA in aqueous.	11
Scheme 3.3 Synthesis of DPAdCage.	12
Scheme 3.4. Proposed DPAdCage photolysis.	22
Scheme 4.1 Synthesis of DAPdeCage	28
Scheme 4.2 Proposed DAPdeCage photolysis scheme.	37
Scheme 5.2 Synthesis of XDAPdeCage	41

I. Introduction: Zinc Homeostasis and Signaling

1.1 Zinc in Biological Systems

Of all trace element metals found in humans, zinc is second abundant after iron^[1]. It can be found in all body tissues as well as secretions, with a distribution of 85% in muscle and bones, 11% in skin and liver, and 4% in other tissues^[2]. On cellular level, the majority cytosolic zinc binds to proteins, enzymes, nucleic acids and other biomolecules. It is estimated that 82% of protein-bound zinc are tetrahedrally coordinated while others are either pentahedrally or hexahedrally coordinated^{[3][4]}. The remaining zinc is labile and often described as “free zinc” in a variety of literatures. It should be noted, however, that free zinc is not ligand-absent, but the interaction is weak and hard to be identified.

The resting free zinc concentrations in different Eukarya cells are estimated to be picomolar^{[5][6][7]}, while the overall zinc in human cells are measured to be around 200~300 μM ^[8]. This significant difference between bound and free zinc ions is attributed to the cellular homeostatic regulation of metal buffering and muffling. The concept of zinc buffering is similar to hydrogen ion (proton) buffering^[7]. Analogous to pH, pZn is used to describe the physiological zinc potential. The value of pZn is determined by the K_d of the buffering ligand therefore reflects its affinity to zinc. When the buffering capacity is strong, the transiently increased zinc concentration will return fast to those at rest. When the buffering capacity is weak, a new steady-state will be reached instead.

Extracellular zinc can be loaded into cells and into subcellular compartments, intracellular zinc, on the other hand, can move in an opposite direction. This time-depended process modulates the non-steady state changes in cytosolic free zinc ions and is termed as “muffling”^{[9][10]}. By removing surplus zinc from a particular location, such as the cytoplasm, cells are enabled with higher zinc uptake. Therefore, zinc muffling process contributes to an increase of the cellular zinc buffering capacity. The transfer of zinc among different cellular compartments requires a large number of transporters. So far, 10 members of zinc transporter (ZnT) family as well as 14 members of the Zrt-irt-like protein (ZIP) family have been

identified and analyzed. They are responsible for cytosolic zinc trafficking and directly affect the muffling ability.

1.2 Zinc Signaling

Under certain physiological conditions, zinc transient triggers signaling. Based on the location of where this happens, the corresponding signal transduction is classified into extracellular zinc signaling and intracellular zinc signaling^{[11][12][13]}. In extracellular zinc signaling, zinc is released from cells in a membrane-mediated manner and acts as a ligand of the receptors expressed on the target cell membranes^{[11][12]}. The extracellular zinc signaling is extensively investigated in the CNS, especially the hippocampal mossy fibers, where zinc is uploaded by ZnT3 into the synaptic vesicles and released from the presynaptic terminals into the synaptic clefts. The secreted zinc performs as a neurotransmitter and mediates the activity of postsynaptic receptors such as NMDA/AMPA receptor, GABA receptor and ZnR/GPR39 (Fig 1.1).

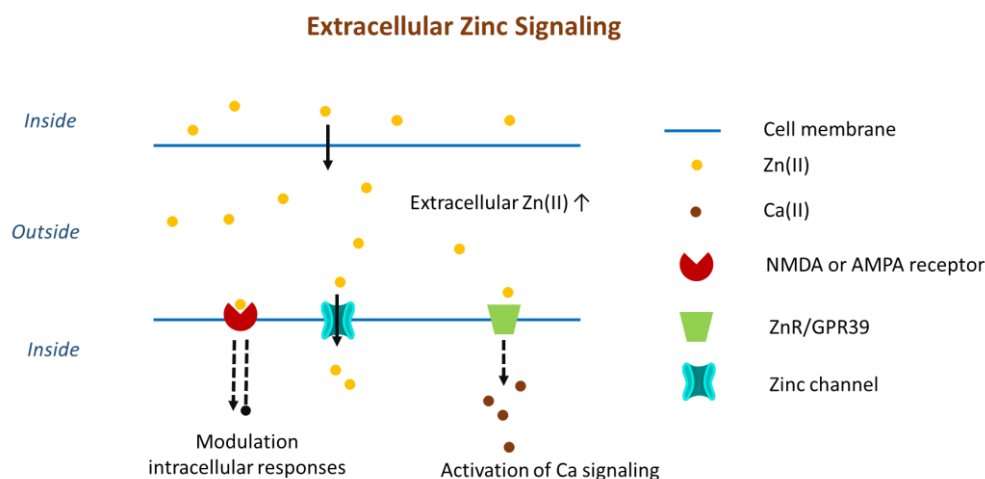


Fig 1.1 Extracellular zinc signaling

The other type of zinc signaling is triggered by extracellular stimuli such as hormones, growth factors and cytokines at the cell surface^[11]. The resulted zinc transient occurs in the cytosol, and the signaling event is therefore called intracellular signaling. In such case, zinc

serves as a second messenger akin to calcium. Based on the timescale in which the zinc signals operate, the intracellular signaling is further classified into two types: fast/early zinc signaling (EZS) and late zinc signaling (LZS)^[14]. EZS is transcription-independent and can be accomplished within seconds to a few minutes, while LZS requires the transcription of zinc transport proteins and lasts for hours. Two examples of such signaling pathways are TLR-4 signaling and FcεRI signaling.

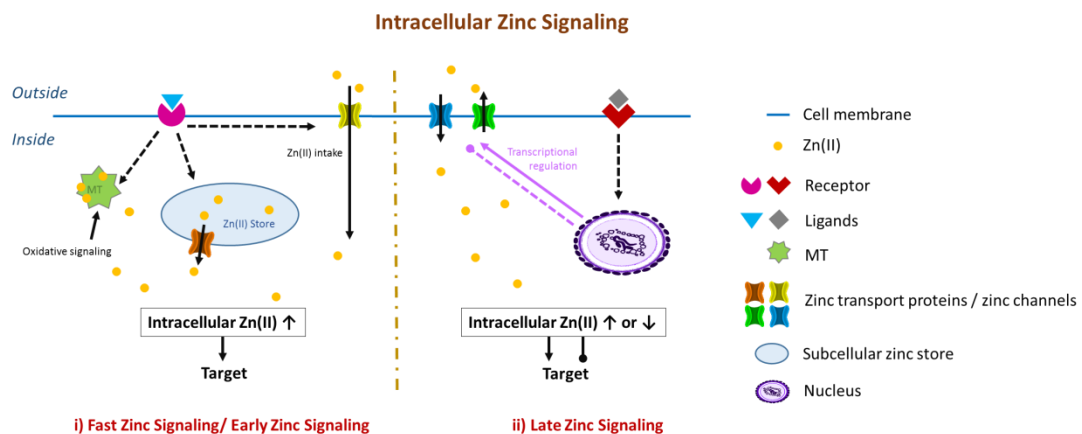


Fig 1.2 Intracellular zinc signaling

In mammals, the cell cycle arrest at metaphase II (MII) of meiosis is considered as a key step in oogenesis. This arrest is stimulated upon fertilization and catalyzed by a series of calcium oscillations that activate downstream molecular targets^{[15][16]}. The influence of zinc on eukaryocyte cell cycle was first discussed about thirty years ago^{[17][18]}. Recently, O’Halloran and his group reported a significant zinc uptake by mouse oocyte during maturation^[19]. Immediately after calcium oscillations upon fertilization, the zinc-enriched egg triggers the ejection of zinc into the extracellular milieu in a series of coordinated events termed “zinc spark”. It lasts for hours and facilitates cell cycle resumption^[19]. Quantitative mapping of zinc fluxes revealed that these zinc sparks arise from vesicles; the latter undergo dynamic movement during oocyte maturation and exocytosis at the time of fertilization^[20]. Two zinc transport proteins, ZIP6 and ZIP10, are expressed in the cortex and thought responsible for zinc accumulation^[21]. It is also suggested that cumulus cells may have a

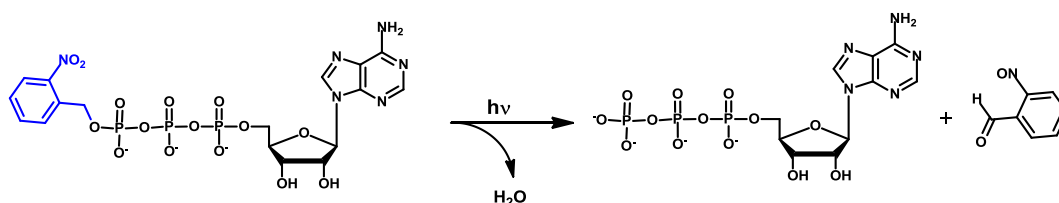
contribution to the complex zinc transport network by forming cumulus-oocyte complex (COC) ^[22].

Zinc spark functions as a late zinc signal and mediates continued egg-to embryo transition^{[13][19]}. The specific molecular mechanism yet remains to be elucidated. It is proposed that zinc exerts concentration-dependent regulation of meiosis through its interaction with EM12, a central component of the cytostatic factor (CSF) ^[23]. EM12 contains a zinc-binding region (ZBR) in its C-terminus that can inhibit the anaphase promoting complex/cyclosome (APC/C) ^{[24][25][26]}. When intracellular zinc arrives a threshold level, it binds ZBR and activates APC/C inhibitor EM12, leading to CSF-mediated MII arrest ^[23]. After activation, the zinc ejection in forms of zinc spark leads to a reduction in cellular zinc and reduced EM12 activity, helping to drive the events of egg activation ^[23].

2 Introduction: Photocages

2.1 Illuminating Cell Chemistry with a Light Switch

Photocages are light sensitive molecules that trap analytes under physiological conditions and release them upon irradiation. The term “cage” was coined by Kaplan, Forbush and Hoffman in 1978 to describe a nitrobenzyl-protected adenosine triphosphate (ATP) in their kinetic studies of ATPase^[27]. In the study, the active site of ATP was blocked by covalent link of the *o*-nitrobenzyl (*o*-NB) group. Illumination initiated a photoreaction of *o*-NB chromophore which caused bond broken and ATP release (Scheme 2.1). Following this idea, a variety of photocages targeted at bioactive molecules including neurotransmitters, nucleotides, peptides, proteins as well as metal ions have been developed and applied in biological and physiological studies^{[28][29][30]}. In practice, the uncaging strategy is considered to be "optically orthogonal" with fluorescence spectra: the former triggers a specific chemical event, and the latter allows observation of such event.



Scheme 2.1 Photolysis of *o*-NB caged ATP. This is the first case of a "caged" molecule.

The distinguished feature of photocages is that it can provide temporal control of cellular chemistry. The uncaging process is actually a photoreaction which decomposes the caged complex apart. This could be either a covalent bond broken or a conformational change, rendering the protected functional site of analyte to be uncovered after photolysis. Since photochemical reactions usually happen very fast accompanied with a release rate within milliseconds, the fast photolysis makes it possible to examine biochemical responses in real time^[31].

Another advantage of photocages is that compared with other techniques, light is relatively easier to operate. Both the direction and the area of irradiation can be modulated, therefore enable the analytes to be released at a specific site -- this could be a number of cells, a single cell or a part of a cell. In addition to spatial control, the level of uncaging can also be achieved by altering the intensity of the light source.

2.2 Photocaged Metal Ion

The idea behind a photocage is that the bioactive site of an analyte can be inhibited by chemical modification with a protecting group. If the analyte is an organic molecules such as neurotransmitters, peptides, proteins and nucleic acids, this inhibition is achieved through a covalent bond that integrates the functional group of the molecule and a photosensitive chromophore. If the analyte is a metal ion, the inhibition is achieved through a three-dimensional coordination between a multi-dentate organic ligand and the central metal ion. Irradiation-triggered photoreaction breaks the interaction between the caging group and the target. In the case of a caged organic molecule, this is a bond broken. In the case of a caged metal ion, this is a formation of a new ligand which has significant diminished metal affinity than before photolysis.

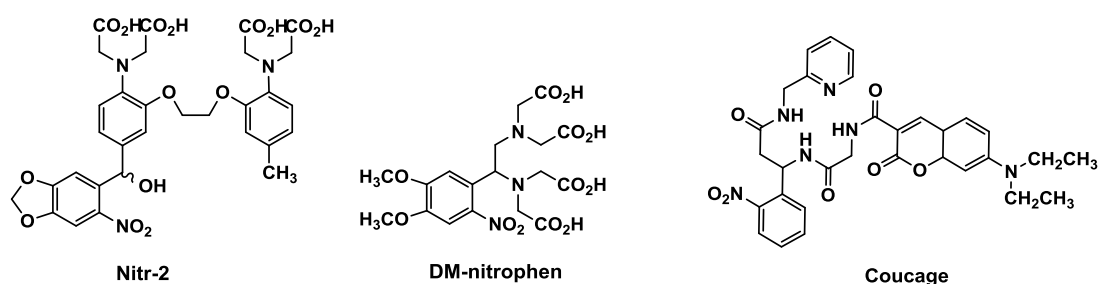


Fig 2.1 Examples of photocages for metal ions. Nitr-5 and DM-nitrophen were designed for caging Ca²⁺, and Coucage were designed for Cu²⁺.

The work of photocaged metal ion was initiated by Roger Tsien and Ellis-Davis in the late 1980s^{[32][33]}. Nitr-5 and DM-nitrophen (Fig 2.1) were among the first developed cages and

have been found successful applications in a wide range of physiological experiments, especially in the investigation of Ca^{2+} mediated signaling transductions^{[34][35][36]}. Following the roadmaps, a variety of other metal cages have also been synthesized for d-block metals such as Cu^{2+} , Zn^{2+} , Fe^{2+} and Fe^{3+} ^{[37]-[41]}.

2.3 Previous Work on Zn^{2+} Photocages

Our group interest is on Zn^{2+} photocages and its application in biological systems. The earlier work attributes to the development of two families: *Cast* and *Cleav*. Two representatives of the *Cast* family are CrownCast and ZinCast-1. CrownCast utilizes a macrocyclic NO_4 ligand as cation receptor and has a 1:1 binding to several alkaline earth metals like Zn^{2+} and Cd^{2+} . The uncaging strategy borrows that of the nitr series reported by Adams and Tsien^[42]. Upon irradiation, the cage undergoes a Norrish-type II photochemical reaction to give nitrosobenzophenone which has a lower metal binding affinity. The reduced affinity results from delocalization of the anilino lone pair onto the benzophenone carbonyl oxygen atom (Scheme 2.2, above)^[42]. ZinCast-1 utilizes a tridentate DPA ligand which more specifically binds to Zn^{2+} and Cu^{2+} ^[43]. It uses the same photochemistry as CrownCast that involves a decreased electron density on a coordinated aniline nitrogen, resulting reduced binding capability (Scheme 2.2, middle)^[43].

ZinCleav-1 is the first member of the ZinCleav family. It utilizes ethylene-bis- α,α' -(2-aminomethyl)pyridine (EBAP) as the chelator and has a significant improved Zn^{2+} affinity ($K_d = 0.23 \text{ pM}$) compared to those reported for ZinCast-1 and its derivatives ($K_d \sim \mu\text{M}$)^[44]. Upon photo irradiation, ZinCleav-1 undergoes an alternative uncaging mechanism that involves a cleavage of the ligand backbone^[44]. The strategy is similar to Ca^{2+} uncaging from DM-Nitrophen reported by Ellis-Davis and is proved to be more efficient than the *Cast* family.

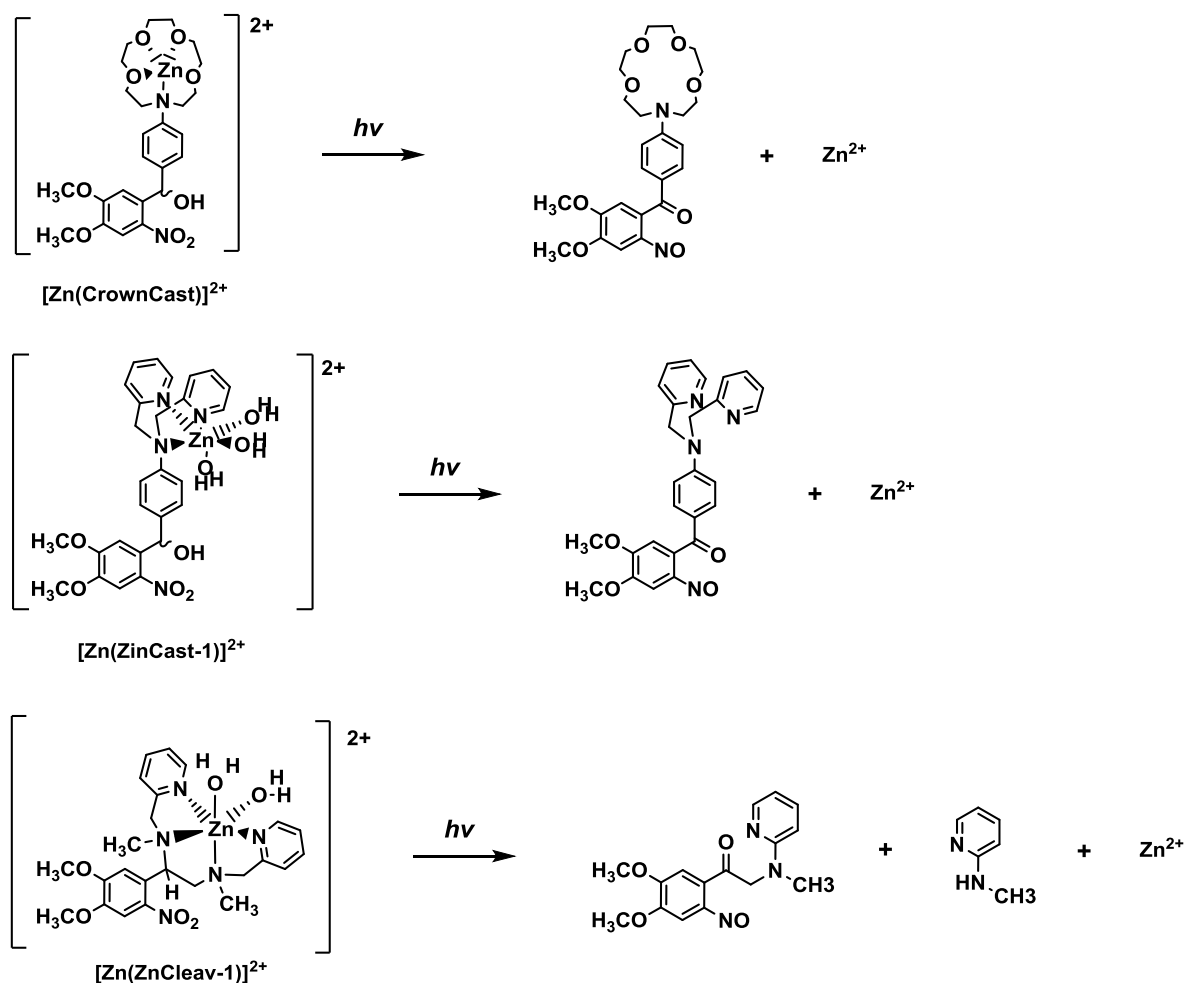


Fig 2.2 Examples of uncaging Zn²⁺ from its photocages. CrownCast and ZinCast-1 are examples of the *Cast* family. ZinCleave-1 is an example of the *Cleave* family.

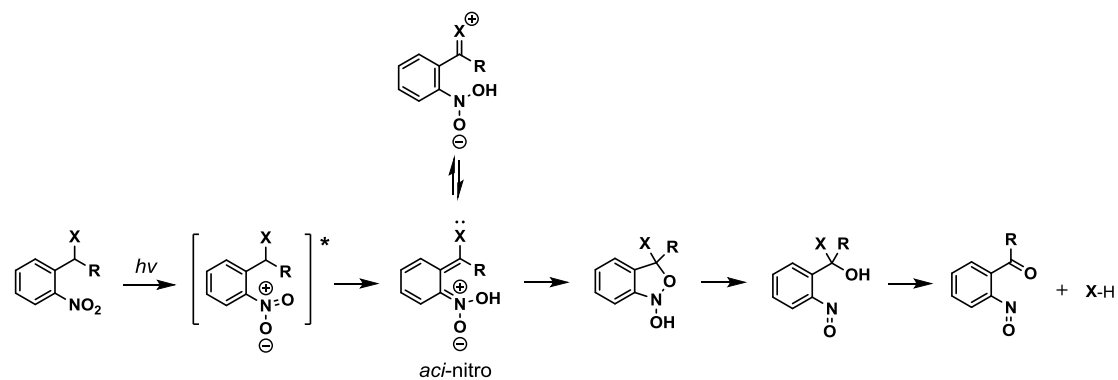
The *Cast* and *Cleave* family includes but not limited to those three photocages noted above. Using ZinCast-1 as a template, we further obtained ZinCast-2, 3, 4, 5 and DiCast-1^[45]. Meanwhile, ZinCleave-2 was also developed as a second generation of ZinCleave-1^[46]. Comparing these cages reveals that the ZinCleavs, especially ZinCleave-2, are more ideal for physiological experiments with relatively high metal binding affinity and uncaging efficiency. All these work as an entirety is considered to be very important approaches for continuing research on new photocages design and their application in a biological system. In addition to the *Cast* and *Cleave*, a more recent accomplishment has been made by our group member, in which a new uncaging strategy based on light-triggered decarboxylation was utilized, and a

new class of Zn^{2+} cages, NTAdCage, has been successfully synthesized and applied to *Xenopus laevis* oocytes^[47]. A further discussion of this photodecarboxylation-driven uncaging can be found in section 3.1.

3 DPAdCage

3.1 Background

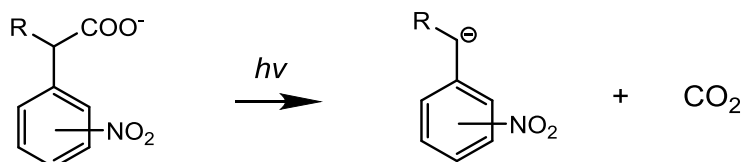
Our previous study of photocaged Zn^{2+} were most focused on two families: *Cast* and *Cleav*. Applying these cages in biological investigations involving Zn^{2+} gives the unique advantage of temporal control of Zn^{2+} fluctuations. Limitations are, however, relatively slow release rate, UV irradiation and formation of reactive nitroso byproducts^[39]. Since most of these drawbacks are associated with the intrinsic photochemistry of *o*-NB group (Scheme 3.1), an alternative uncaging strategy based on photoinduced decarboxylation was explored. The photochemistry involves the formation of a carbon-centered anion on the side chain of a chromophore. The carbanion intermediate has a very short lifetime and promotes a rapid β -elimination, releasing the analyte in its active form (Scheme 3.2)^{[48][49]}. Compared to other traditional uncaging strategies, photodecarboxylation features in its high quantum yields, fast photorelease rates and aqueous compatibility^{[48]-[51]}.



Scheme 3.1 Reaction mechanism of *o*-nitrobenzyl based photolysis.

Benzophenone, xanthone and phthalimide are three chromophores that are commonly used in photodecarboxylation studies^{[52][53][54]}. Nitrophenylacetate (NPA) is also reported to undergo a fast photolysis accompanied with the formation of CO_2 in aqueous solutions (Scheme 3.2)^[48]. Enlightened by the decarboxylation mechanism of *meta*-NPA, our group recently reported NTAdCage as a new class of Zn^{2+} cages. The compound integrates a nitrilotriacetate (NTA) receptor and an *m*-NPA chromophore together and has a moderate binding affinity, high quantum yields and less cytotoxicity^[47]. Bis(2-pyridylmethyl)glycine

(BPG) is also a tetradentate tripodal ligand for Zn^{2+} ^[55]. It has a higher Zn^{2+} specificity by substituting two of the NTA carboxylate groups with pyridyl groups. To further explore the decarboxylation based uncaging mechanism, here a second generation cage named DPAdCage was designed by integrating BPG ligand to the *m*-NPA chromophore.



Scheme 3.2 Photodecarboxylation of NPA in aqueous.

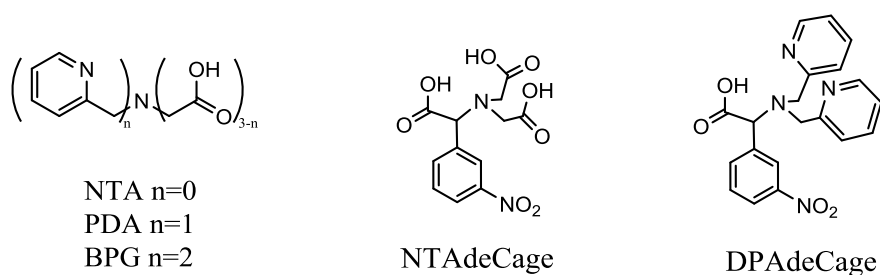


Fig 3.1 Structures of NTA, PDA, BPG and NTAdCage, DPAdCage.

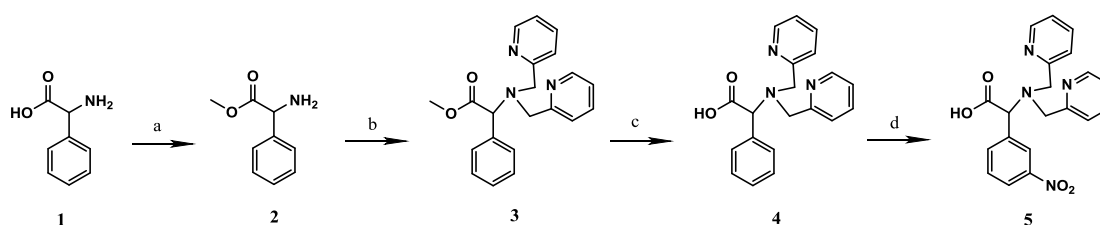
3.2 Experimental Section

3.2.1 Materials and Methods

All reagents were purchased from Acros and Alfa Aesar at the highest commercial quality and used without further purification. Dichloroethane (DCE) were dried before taking to use by a Seca Solvent Purification System. All chromatography and TLC were performed on either silica (230-400 mesh) from Silicycle or Aluminumoxide (basic, 50-200 μ m, 60A) from Acros. TLCs were developed using mixtures of ether/hexanes, CH_2Cl_2 /hexanes, ethyl acetate (EA)/hexanes and CH_2Cl_2 / CH_3OH and were visualized with 254 or 365 nm light. 1H and ^{13}C NMR were obtained using a 500 MHz Bruker NMR instrument, the corresponding

chemical shifts were reported in ppm on the δ scale relative to tetramethylsilane (TMS). IR spectra were recorded on a Bruker Vertex 70 FTIR and the samples were prepared as thin films on KBr plates or pellets. LC/MS was carried on a Single Quadruple, Agilent Technologies 1200 series LC system. High resolution mass spectra were obtained at the University of Notre Dame mass spectrometry facility using microTOF instrument operating in positive ionization mode (+ESI-TOF).

3.2.2 Synthetic Procedures



Scheme 3.3 Synthesis of DPAdCage.

2-Amino-2-phenylacetic acid (2). To a 250 mL round bottomed flask L-(+)-2-phenylglycine (4.53 g, 30 mmol) was added in CH_3OH (40 mL). With stirring, concentrated H_2SO_4 (8 mL) was added and the mixture was refluxed for 2.5 h. The excess CH_3OH was removed and 20 mL of H_2O was added to the residue in an ice bath. The aqueous solution was neutralized using saturated Na_2CO_3 and the product was extracted into ethyl acetate (3×20 mL). The combined organics were dried over anhydrous Na_2SO_4 , filtered, and the solvent was removed on a rotary evaporator to yield **2** as a colorless oil (3.43 g, 69.2%). ^1H NMR and ^{13}C NMR are in good agreement with those reported^[47].

Methyl 2-(bis(pyridin-2-ylmethyl)amino)-2-phenylacetate (3). To a 100 mL round bottomed flask was added compound **2** (1.03 g, 6.24 mmol) and 2-pyridinecarboxaldehyde (1.30 mL, 13.7 mmol) in 1,2-dichloroethane (20 mL). The mixture was brought to reflux for 1 h and then allowed to cool down to room temperature. $\text{NaBH}(\text{OAc})_3$ (3.30 g, 15.6 mmol) was added and the resulting mixture was further stirred for an additional 18 h. Water (20 mL) was

added and the product was extracted into CH₂Cl₂ (3 × 10 mL). The organic layers were combined, dried over anhydrous Na₂SO₄, filtered, and the solvent was removed on a rotary evaporator. Flash chromatography on alumina (CH₂Cl₂) yielded **3** as a yellow oil (617 mg, 28.5%). ¹H NMR (CDCl₃) δ 8.49 (d, J = 4.9 Hz, 2H), 7.62 (td, J = 7.6, 1.8 Hz, 2H), 7.50 (d, J = 7.9 Hz, 2H), 7.41 – 7.39 (m, 2H), 7.36 – 7.32 (m, 2H), 7.31 – 7.27 (m, 1H), 7.11 (t, J = 6.7 Hz, 2H), 4.74 (s, 1H), 4.07 (d, J = 14.5 Hz, 2H), 3.89 (d, J = 15.2 Hz, 2H), 3.75 (s, 3H). ¹³C NMR (CDCl₃) δ 172.7, 160.0, 149.1, 136.5, 136.2, 129.1, 128.6, 128.2, 123.1, 122.1, 67.6, 57.0, 51.9. HRMS calc. 348.1693, found 348.1706.

2-(Bis(pyridin-2-ylmethyl)amino)-2-phenylacetic acid (4). To a 20 mL glass vial compound **3** (405 mg, 1.16 mmol) was dissolved in CH₃OH (2 mL). NaOH (464 mg, 11.6 mmol) in H₂O (500 μL) was carefully added. The mixture was stirred under room temperature for 16 h and the solvent was removed under reduced pressure. A small portion of H₂O was added and the aqueous pH was adjusted to 5. The product was extracted into CH₂Cl₂ (3 × 10 mL) from aqueous. The organic extracts were combined and dried over anhydrous Na₂SO₄, filtered, and the solvent was removed under reduced pressure to give a white solid **4** (135 mg, 34.9%); mp= 97– 99 °C. ¹H NMR (CDCl₃) δ 8.58 (d, J = 4.9 Hz, 2H), 7.57 (td, J = 8.5, 1.7 Hz, 2H), 7.34 – 7.28 (m, 5H), 7.18 – 7.16 (m, 2H), 7.14 – 7.12 (d, J = 7.7 Hz, 2H), 4.87 (s, 1H), 3.97 (d, J = 15.2 Hz, 2H), 3.80 (d, J = 15.4 Hz, 2H). ¹³C NMR (CDCl₃) δ 174.5, 158.8, 148.7, 137.3, 135.6, 129.7, 128.8, 128.4, 123.1, 122.7, 70.4, 56.9. HRMS calc. 334.1571, found 334.1550

2-(Bis(pyridin-2-ylmethyl)amino)-2-(3-nitrophenyl)acetic acid (DPAdCage, 5). Compound **4** (97 mg, 0.29 mmol) was added to concentrated H₂SO₄ (2 mL) and stirred for 10 min. HNO₃ (70%, 300 μL) was carefully added in the dark. The reaction was kept at below 0 °C using a CH₃CN/dry ice bath for 1.5 h. Crushed ice was added to the mixture after the reaction is finished and the pH was adjusted to 5. The product was extracted into ethyl acetate (3 × 10 mL) from aqueous. The combined organic layers were dried over anhydrous Na₂SO₄ and filtered. The solvent was removed on a rotary evaporator to yield **5** as a yellow powder (31 mg, 28%). mp= 97– 99 °C. ¹H NMR (CDCl₃) δ 8.58 (d, J = 4.9 Hz, 2H), 7.57 (td, J = 8.5, 1.7 Hz, 2H), 7.34 – 7.28 (m, 5H), 7.18 – 7.16 (m, 2H), 7.14 – 7.12 (d, J = 7.7 Hz, 2H), 4.87

(s, 1H), 3.97 (d, J = 15.2 Hz, 2H), 3.80 (d, J = 15.4 Hz, 2H). ¹³C NMR (CDCl₃) δ 174.5, 158.8, 148.7, 137.3, 135.6, 129.7, 128.8, 128.4, 123.1, 122.7, 70.4, 56.9. FT-IR (neat, cm⁻¹) 3061.1, 2843.2, 2325.3, 2161.3, 2051.5, 1980.0, 1700.9, 1592.2, 1570.5, 1494.6, 1474.5, 1434.8, 1367.9, 1223.5, 1185.4, 1143.0, 1094.7, 1049.5, 1031.2, 1019.7, 1002.8, 995.1, 977.4, 902.4, 838.7, 762.4, 700.1, 667.4, 638.9, 617.0.

General Spectroscopic Methods

All solutions were prepared using spectroscopic grade solvents or Millipore (Biopak™ Ultrafiltration Cartridge) water. HEPES (4-(2-hydroxyethyl)-1-piperazineethanesulfonic acid), and KCl (99.8%) were bought from Fisher Scientific used without further purification. The pH values were recorded with Acumet pH glass electrode that was calibrated prior to use. Zn²⁺ stock solution was prepared from ZnCl₂ and standardized by titrating with terpyridine. DPAdCage stock solution was prepared in DMSO or CH₃OH at 10 mM before introducing to aqueous. All the spectroscopic experiments were performed and recorded at 25 °C. Absorption spectra were recorded on a Thermo Scientific Evolution 300 UV-vis spectrometer using Cary winUV software and the samples were placed on a 1.0 cm quartz cuvette. Fluorescence spectra were recorded on a Hitachi F-4500 spectrometer controlled by Pentium-IV PC run by FL solutions 2.0 software package. A 150 W Xe arc lamp (Ushio Inc.) operating at 5 A (current), 700 V was used for excitation and the samples were placed on a 1.0 cm quartz cuvette. LC-MS was carried on a Agilent Technologies 1200 series LC system and the traces at 254 nm was recorded for analysis. Ketoprofen (0.8 mM) was used as internal standard and all the samples were eluted with an isocratic mixture of 95:5 CH₃CN:H₂O containing 0.1% formic acid at a flow rate of 0.3 mL/min.

3.2.3 Determination of Zn²⁺ Binding Affinity

A 2.0 mL of 200 μM 4-(2-pyridylazo)resorcinol (PAR) was prepared in aqueous buffer (40 mM HEPES, 100 mM KCl, pH 7.0) in a quartz cuvette. A 2.0 μL aliquot of ZnCl₂ (10 mM) was added and the UV spectrum were recorded before and after adding Zn²⁺. The solution was titrated with DPAdCage (2.0 mM) in 2.0 μL increments and the spectra were recorded after each titration. To ensure reproducible results, the procedure was repeated in

triplicate. The binding equilibrium was expressed as equation 1 and the binding constant (K') of the $[\text{Zn}(\text{DPAdCage})]^+$ was calculated using equation 2, where $\beta'_{\text{PAR}} = 2.2 \times 10^{12} \text{ M}^{-1}$ and $\Delta\varepsilon_{500} = 6.6 \times 10^4$ [56].



$$\frac{[\text{Zn}(\text{DPAdCage})][\text{PAR}]^2}{[\text{DPAdCage}][\text{PAR}_2\text{Zn}]} = \frac{K'}{\beta'_{\text{PAR}}} \quad (2)$$

$$[\text{PAR}_2\text{Zn}] = \frac{A_{500}}{\Delta\varepsilon_{500}} \quad (3)$$

$$[\text{PAR}] = [\text{PAR}]_{\text{total}} - 2[\text{PAR}_2\text{Zn}] \quad (4)$$

$$[\text{Zn}(\text{DPAdCage})] = [\text{PAR}_2\text{Zn}]_{\text{initial}} - [\text{PAR}_2\text{Zn}] \quad (5)$$

$$[\text{DPAdCage}] = [\text{DPAdCage}]_{\text{total}} - [\text{Zn}(\text{DPAdCage})] \quad (6)$$

K' was calculated at each data point, averaged and corrected for ligand protonation using pKa values reported for BPG [55]. The corrected binding constant was used to calculate the dissociation constant (K_d) of the $[\text{Zn}(\text{DPAdCage})]^+$ complex.

3.2.4 Determination of Quantum Efficiency

Calibration. A series of DPAdCage solutions at different concentrations (0.2 mM, 0.6 mM, 1 mM, 1.4 mM, 1.8 mM, 2.2 mM) were prepared in HEPES (pH 7.5) from a 10 mM stock. The samples were injected into LC-MS and the LC traces of each solution were recorded. The area of the peak was determined by integration and its relationship with concentration was calculated. The $[\text{Zn}(\text{DPAdCage})]^+$ was calibrated in a same way.

Photolysis of DPAdCage and $[\text{Zn}(\text{DPAdCage})]^+$. A 3.0 mL solution of 2.0 mM DPAdCage (40 mM HEPES, 100 mM KCl, pH 7.5) was prepared in a quartz cuvette. The sample was irradiated using a LED UV light (365 nm, 3 W) for 10 s and its LC traces was recorded. The procedure was repeated by irradiating samples for 20 s, 30 s and 40 s. The area of the DPAdCage peak was determined by integration and the concentration was calculated from the calibration curve. The corresponding quantum efficiency was calculated from equation 7, where the intensity of the light source was determined using potassium ferrioxalate actinometry [44]. The measurement was repeated in triplicate to ensure its

reproducibility. The quantum efficiency of $[\text{Zn}(\text{DPAdCage})]^+$ was measured in the same way.

$$\text{Quantum Efficiency} = \frac{\Delta[\text{DPAdCage}]/\text{Irradiation time}}{\text{Light Intensity}} \times N_A \quad (7)$$

3.2.5 Release of Caged Zn^{2+}

ZTRS was synthesized following the previously published procedure^[57] and its stock solution was prepared freshly in CH_3OH . A 2.0 mL of 10 μM ZTRS solution (40mM HEPES, 100 mM KCl, pH 7.5) was prepared in a quartz cuvette and its emission spectrum was recorded. A 1 μL aliquot of 20 mM ZnCl_2 was added to this cuvette and its spectrum was recorded. To another cuvette, a 2.0 mL solution containing 10 μM ZTRS, 1 eq of Zn^{2+} and 4 eq of DPAdCage was prepared and its spectrum was recorded. The changes in emission spectra upon zinc release was recorded by preparing a series of solutions each containing 2.0 mL of 10 μM Zn^{2+} with 4 eq of DPAdCage and irradiating at 365 nm for 30 s, 60 s, 90 s...separately. A 10 μL aliquot of 2 mM ZTRS was added to each of the solutions and the corresponding spectra were recorded.

In the another experiment, a solution of 5 μM $[\text{Zn}(\text{DPAdCage})]^+$ containing 10 μM PAR was prepared in a quartz cuvette and its UV spectrum was recorded. The sample was irradiated at 365 nm and the spectrum was recorded. A rise in absorbance at 500 nm was observed, indicating the formation of Zn-PAR complex. As a control, a 10 μM PAR solution prepared in the same cuvette was irradiated in the same way and the UV spectra were recorded before and after irradiation.

3.2.6 Metal Selectivity

Ca-Zn exchange. To a quartz cuvette a 2.0 mL buffer (HEPES, pH 7.5) containing 20 μM DPAdCage, 10 μM Zn^{2+} and 10 μM PAR was prepared and its UV spectrum was recorded. The solution was titrated with an increasing amount of CaCl_2 and the spectra were recorded for each titration.

Cu-Zn exchange. A 50 μM $[\text{Zn}(\text{DPAdCage})]^+$ was prepared in a quartz cuvette and its UV spectrum was recorded. 0.25 eq, 0.5 eq, 0.75 eq, 1 eq aliquots of CuCl_2 was added and the mixture was stirred for 1 min before spectrum was recorded. In another cuvette, a 50 μM DPAdCage was prepared and 1 eq aliquots of CuCl_2 was added, the spectrum was recorded.

3.3 Results and Discussion

3.3.1 Design and Synthesis

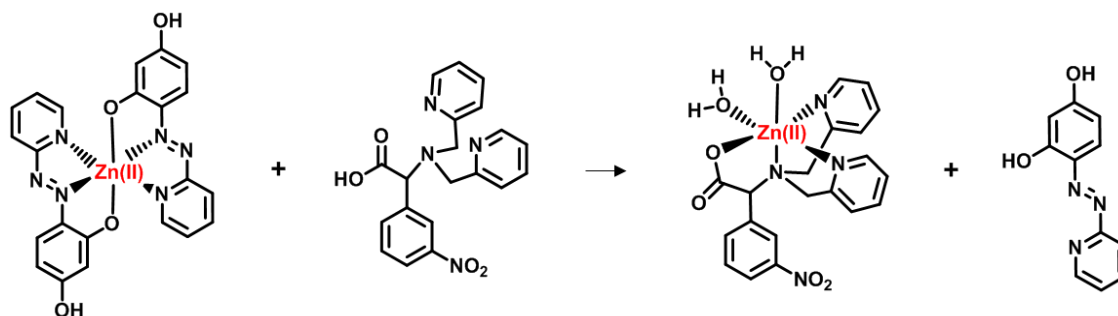
The initial design of DPAdCage was based on *N,N*-bis(2-picolyl)glycine (BPG), a tetradentate chelator which has a pM affinity for Zn^{2+} ^{[55][58]}. Synthesis of DPAdCage started from esterification of the commercially available L-phenyl glycine to get compound **2**. This was followed by a combined two-step reduction in which the alkyl pyridine ligands were introduced to give **3**. Hydrolysis of compound **3** yielded **4**, which had the desired BPG ligand cooperated to benzene. The nitro group was introduced in the last step to avoid unnecessary handling and manipulation of photoactive compounds during the synthesis.

3.3.2 Zn^{2+} Binding Studies

The Zn-DPAdCage complex lacks spectroscopic signature. To measure the binding affinity, a reported competitive titration strategy previously used to study ZinCleave-1 and NTAdCage was employed^{[44][47]}. 4-(2-Pyridyl-2-azo) resorcinol (PAR), a well-known metallochromic indicator for Zn^{2+} , forms a 2:1 complex when PAR is in sufficient excess and a 1:1 complex when it is opposite^[56]. Here an excess amount of PAR (> 10 fold, compared to Zn^{2+}) in solution was prepared to ensure a complete formation of PAR_2Zn complex. PAR_2Zn has a λ_{max} at 500 nm, therefore by monitoring the absorbance changes at this wavelength upon competitive titration by DPAdCage, it gives information about Zn^{2+} depletion from PAR_2Zn complex due to a preferred Zn-DPAdCage binding. The binding constant (K') of $[\text{Zn}(\text{DPAdCage})]^+$ was calculated using equation 2 while the relative components were calculated using equation 3-6. The volume changes upon DPAdCage addition were adjusted to calculate the concentrations and the ligand protonation was also considered for correction.

It is suggested that at physiological conditions (pH 7.0), the Zn-DPAdeCage has a measured K_d of ~ 25.2 μM . This is consistent with its structurally analog BPG, which has a reported K_d of 3.98 μM ^[55]. Since Zn^{2+} binds to di-(2-picolyl) amine (DPA) at 158 nM ^[59], a moderate ΔK_d of ~ 10000 is suggested upon photolysis $[\text{Zn}(\text{DPAdeCage})]^+$ complex.

a)



b)

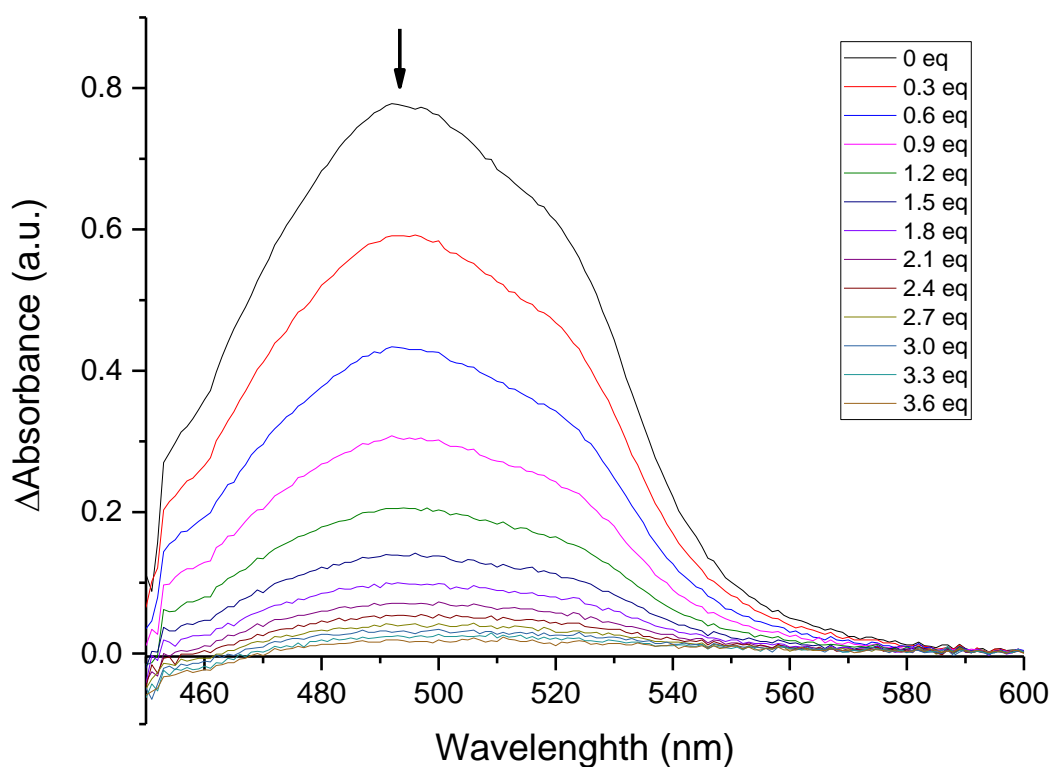
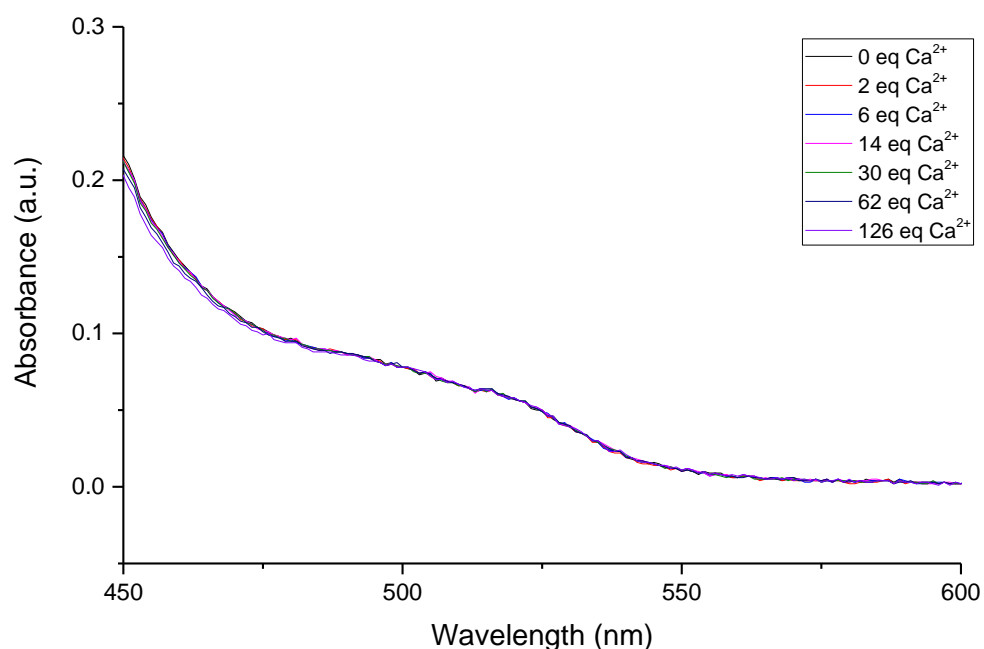


Fig 3.2 Competitive titration between DPAdeCage and PAR in the presence of Zn^{2+} . A solution of 200 μM PAR and 10 μM Zn^{2+} (40 mM HEPES, 100 mM KCl, pH 7.0) was titrated against a stock solution of DPAdeCage (2.0 mM) and the UV absorbance spectrum was recorded after each addition.

The λ_{\max} at 500 nm is attributed to the absorbance of PAR_2Zn . Adding DPAdCage causes Zn^{2+} depletion from Zn-PAR complex and this is evidenced by a decreasing of the absorbance.

The DPAdCage has a carboxyl group. A potential ion exchange of $[\text{Zn}(\text{DPAdCage})]^+$ in the presence of excess Ca^{2+} was studied by titrating CaCl_2 solution to a mixture of $[\text{Zn}(\text{DPAdCage})]^+$ and PAR (Fig 3.3, a). In the presence of 1.26 mM Ca^{2+} , no formation of PAR_2Zn complex was observed, indicating an insignificant Zn^{2+} displacement at typical Ca^{2+} resting levels. The other similar study of Cu-Zn exchange was conducted by adding 1 eq Cu^{2+} directly to $[\text{Zn}(\text{DPAdCage})]^+$ solution (Fig 3.3, b). While an uncompleted slow Cu-Zn exchange was observed, consistent with the Irving-Williams series. Since the resting Cu^{2+} at cellular level is much lower than Zn^{2+} therefore we propose the displacement should not be a worry.

a)



b)

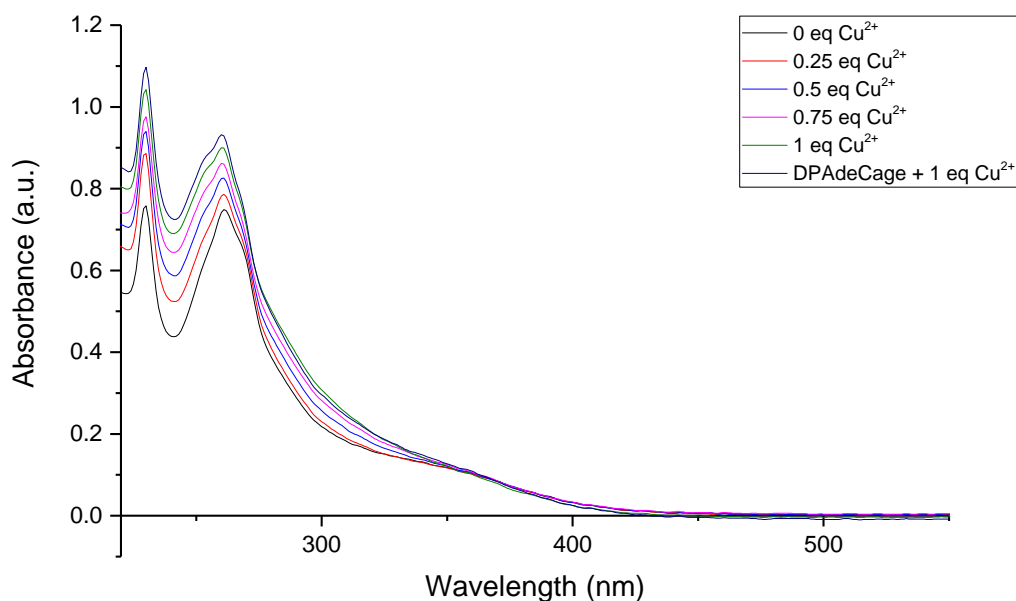


Fig 3.3. a) Non-observable Ca-Zn exchange. A mixture of 20 μM DPAdCage, 10 μM ZnCl_2 and 10 μM of PAR solution was titrated with an increasing amount of CaCl_2 . The absorbance at 500 nm was tracked to see if PAR_2Zn formed. b) Cu-Zn exchange. A mixture of 50 μM DPAdCage and 50 μM ZnCl_2 solution was prepared and titrated with 0.25, 0.5, 0.75, 1 eq of CuCl_2 . In another cuvette, a 50 μM DPAdCage was prepared and 1 eq of CuCl_2 was added, the spectrum was recorded.

3.3.3 Photochemistry

The photoactivity of DPAdCage was analyzed by its quantum efficiency at 365 nm (LED, 3W). The breakage of the cage upon irradiation was tracked by LC-MS and the disappearance of DPAdCage over time was used to determine the quantum efficiency (equation 7). The quantum efficiency of DPAdCage and $[\text{Zn}(\text{DPAdCage})]^+$ were calculated to be 39% and 7.1% respectively, indicating an improved efficient photolysis reaction compared to those *o*-NB derivatives based on a cleavage mechanism. Further analysis of the mass spectra indicated the formation of *m*-nitrobenzaldehyde (*m*-NB) and DPA. To confirm this, commercially obtained *m*-NB and DPA were injected into LC-MS instrument. Their retention time on LC traces as well as the mass spectra were compared to those obtained from the previously photolyzed samples. A perfect match of both retention time and *m/z* values

suggested that upon irradiation, the DPAdCage undergoes an efficient decarboxylation which forms *m*-NB and DPA as major photoproducts. In addition, the appearance of the peak at ~6.1 min (Fig 3.4 and Fig 3.5, c) suggested a possible different pathway which results the formation of a nitrobenzamide, predicted as 3-nitro-*N,N*-bis(pyridin-2-ylmethyl)benzamide (NBPB), based on its *m/z* value. To confirm this, a two-step synthesis was carried out starting with benzoyl chloride and DPA and the hypothesized photoproduct, 3-nitro-*N,N*-bis(pyridin-2-ylmethyl)benzamide, was prepared and injected into LC-MS. The hypothesis was confirmed by comparing the retention time and *m/z* value as earlier described.

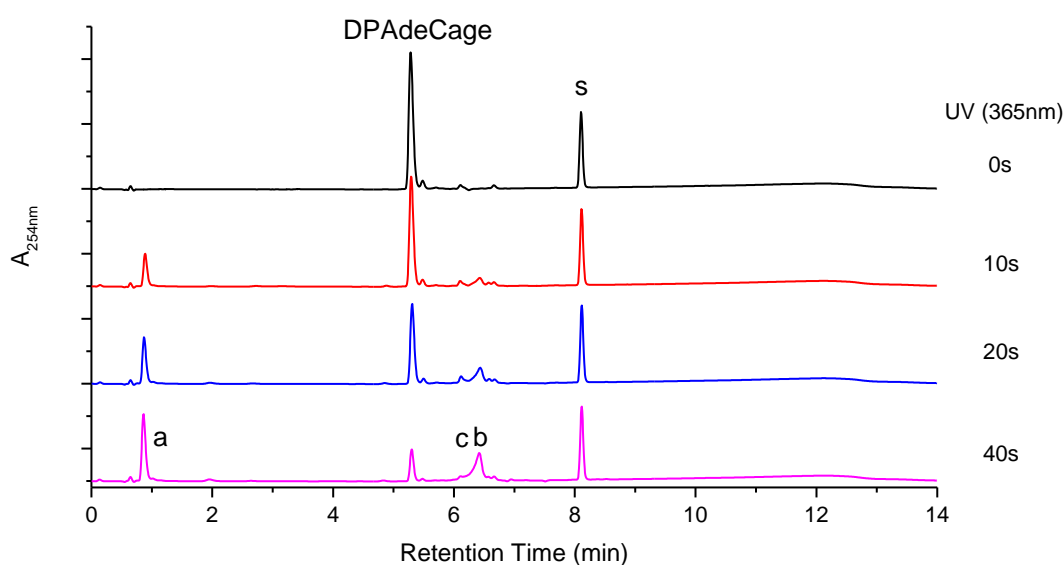


Fig 3.4. LC traces of DPAdCage (2 mM, 40 mM HEPES, 100 mM KCl, pH 7.5) before and after irradiation at 365 nm. Ketoprofen (s) was used as internal standard. A disappearance of DPAdCage accompanied with an appearance of major photoproducts (DPA, a; *m*-nitrobenzaldehyde, b) and minor photoproduct (3-nitro-*N,N*-bis(pyridin-2-ylmethyl)benzamide, c) was observed.

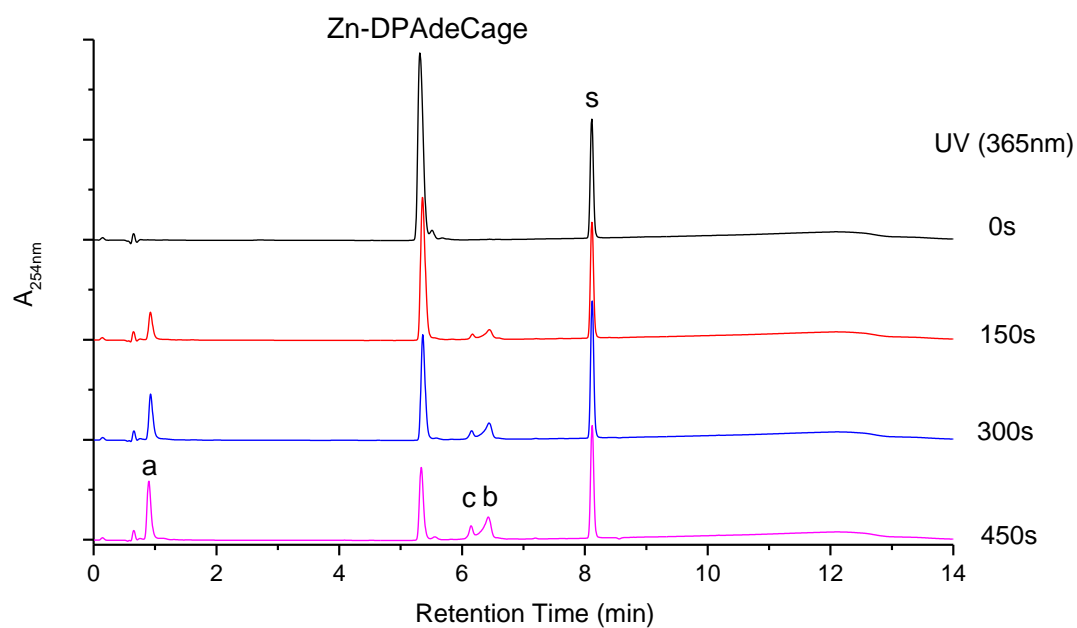
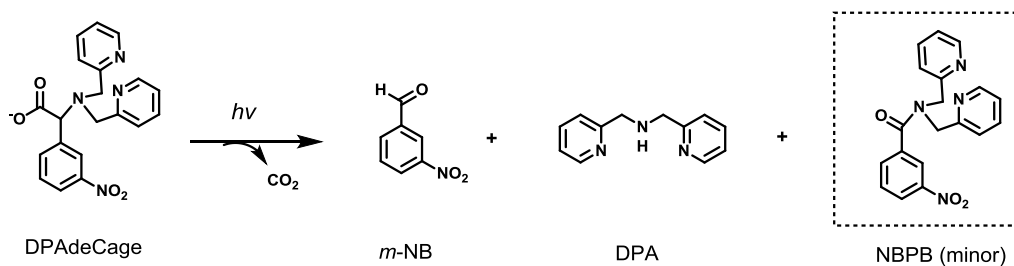


Fig 3.5. LC traces of $[\text{Zn}(\text{DPAdeCage})]^+$ (1 mM, 40 mM HEPES, 100 mM KCl, pH 7.5) before and after irradiation at 365 nm. Ketoprofen (s) was used as internal standard. A disappearance of $[\text{Zn}(\text{DPAdeCage})]^+$ accompanied with an appearance of major photoproducts (DPA, a; *m*-nitrobenzaldehyde, b) and minor photoproduct (3-nitro-*N,N*-bis(pyridin-2-ylmethyl)benzamide, c) was observed.

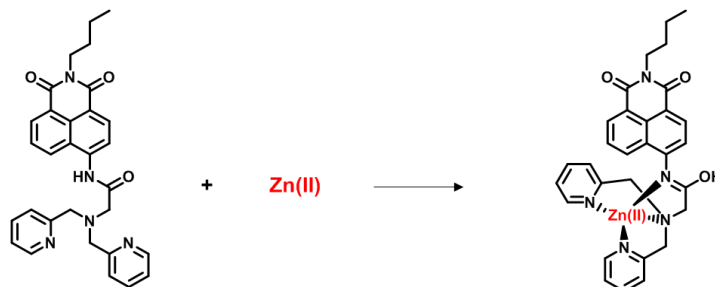


Scheme 3.4. Proposed DPAdeCage photolysis.

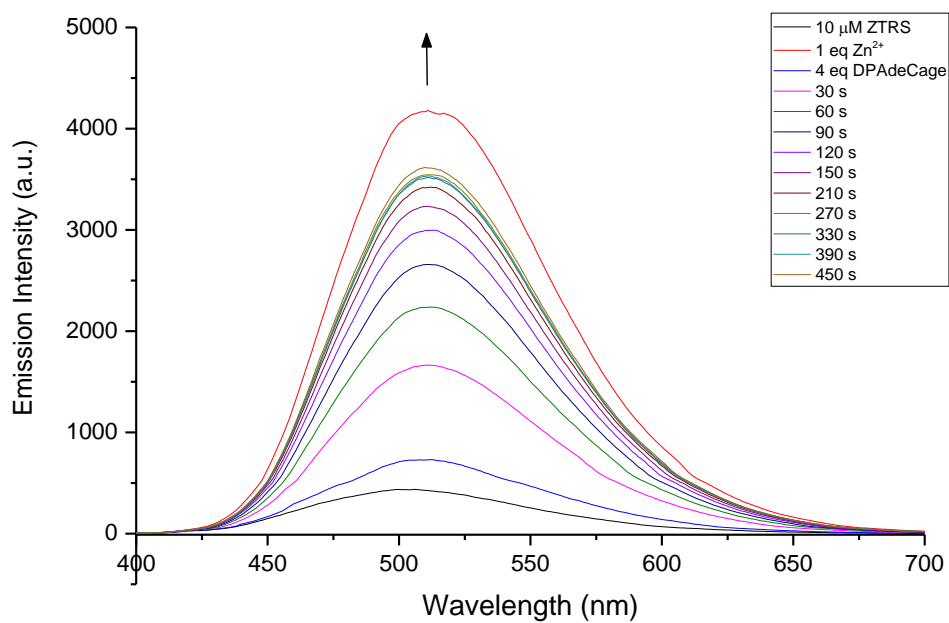
The release of caged Zn^{2+} was further accessed by uncaging the complex in a quartz cuvette and monitor the released free Zn^{2+} using a fluorescent sensor. ZTRS, which has a K_d of 5.7 nM, was chosen for its moderate binding affinity to Zn^{2+} in the presence of $[\text{Zn}(\text{DPAdeCage})]^+$ (before photolysis) and DPA (after photolysis). Prior to experiment, the

dynamic ligand exchange was simulated using HySS^[60], in which different ratios of the species (Zn^{2+} , DPAdCage, DPA) were modulated to obtain a best condition (10 μM ZTRS, 1 eq of Zn^{2+} and 4 eq of DPAdCage). To avoid photo bleaching, a series of caged Zn^{2+} samples were prepared under the same condition but irradiated for different seconds, and ZTRS was added to each sample after photolysis. Results showed that addition of 40 μM DPAdCage to a solution of 10 μM $[\text{Zn}(\text{ZTRS})]^{2+}$ causes an immediate extinguish of fluorescence at 512 nm which was observed when $[\text{Zn}(\text{ZTRS})]^{2+}$ formed, indicating the equilibrium shifted to form a new non-fluorescent complex, $[\text{Zn}(\text{DPAdCage})]^+$. Irradiating $[\text{Zn}(\text{DPAdCage})]^+$ at 365 nm for about 5 min causes a restoration of the fluorescence, indicating the breakage of high affinity Zn^{2+} chelator DPAdCage and a successful release of Zn^{2+} (Fig 3.6). The uncaging of Zn^{2+} was further confirmed by UV-vis, where a formation of PAR_2Zn complex at 500 nm was observed during light irradiation (Fig 3.7).

a)



b)



c)

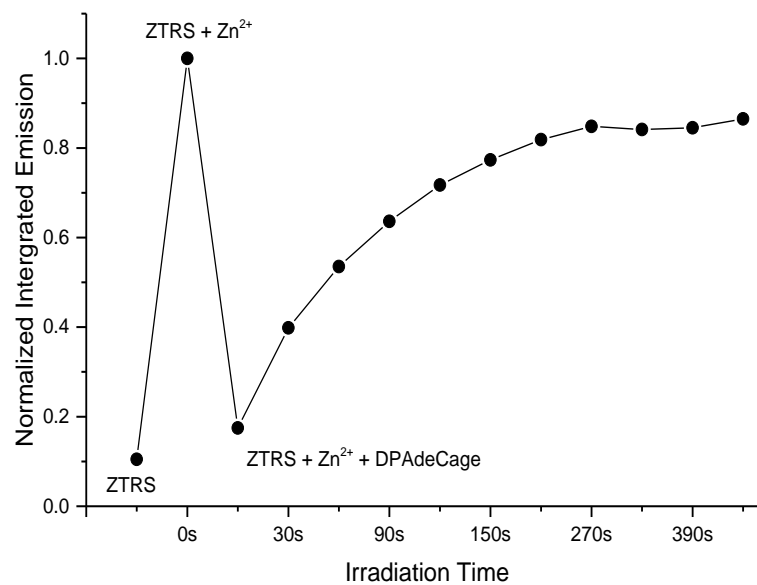
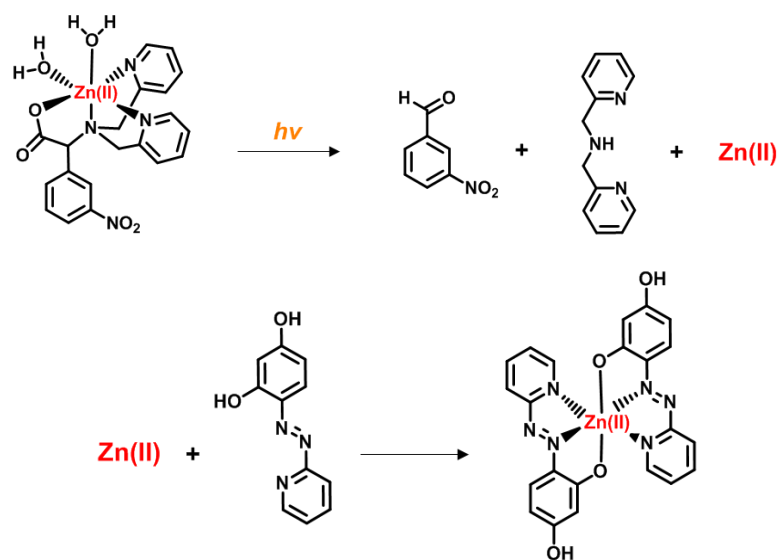


Fig 3.6. a) Formation of Zn-ZTRS. b,c) Fluorescence response of ZTRS upon uncaging of DPAdCage. Emission Intensity of 10 μM ZTRS was recorded before and after 10 μM Zn^{2+} addition. Subsequent 40 μM DPAdCage addition quenched the emission of Zn-ZTRS, while the followed irradiation led to a complete photolysis in ~ 5 min and restored the emission.

a)



b)

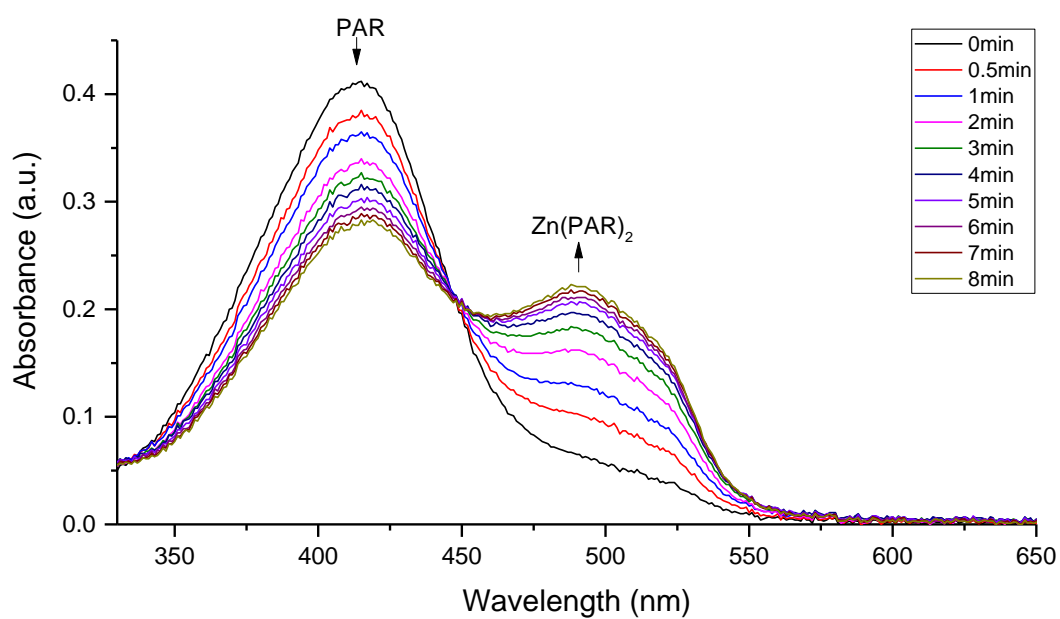
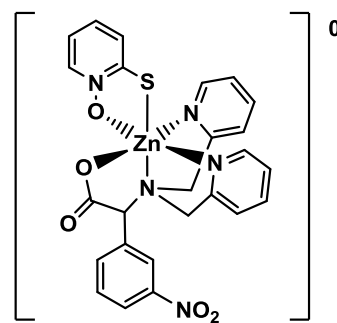


Fig 3.7. Zn²⁺ uncaging tracked by the formation of Zn-PAR complex. A solution of 5 μM [Zn(DPAdeCage)]⁺ containing 10 μM PAR was prepared in a quartz cuvette and its UV spectrum was recorded. The sample was irradiated at 365 nm and the spectrum was recorded. A rise in absorbance at 500 nm was observed, indicating the formation of Zn-PAR complex.

4 DAPdeCage

4.1 Background

At cellular level, the homeostasis of Zn^{2+} is tightly regulated in forms of Zn^{2+} buffering and muffling. Measurements of labile Zn^{2+} in different cells and tissues indicate a resting level between pM to nM^[61]. Meanwhile, an up to 9-order transient increase of free Zn^{2+} can be observed in a signaling event, for example, the generation of "zinc sparks" during oocytes fertilization^{[62][63]}. In order to load the photocaged Zn^{2+} across the cell membrane for intracellular signaling study, it is required that the complex as an entirety has to be charge neutral. The requirement is usually satisfied by structure modification with positively or negatively charged small ligands, depending on the electrical characteristic of the caged complex (Fig 4.1). In a recent biological study done by another graduate in our group, a DPAdCage-Zn-pyrithione complex was prepared and loaded into the cells by passive diffusion. The introduction of pyrithione is to neutralize the extra charge carried by the $[Zn(DPAdCage)]^+$. However, it was also observed to have an interference with the photolysis process, although the reason remains unclear. To avoid



DPAdCage-Zn-Pyrithione

unnecessary operations that may disturb the physiological conditions, ligands with two negative charges were explored. *N*-(2-Pyridylmethyl)iminodiacetic acid (PDA) is also a ternary Zn^{2+} chelator with a moderate pM affinity^[55]. It structurally resembles NTA and BPG and has one pyridyl groups and two carboxylic groups (Fig 3.1). In aqueous solutions, PDA forms a 1:1 complexes with Zn^{2+} ^[55]. The net charge of this complex is zero thus theoretically cell permeable. Based on the successful development of NTAdCage and DPAdCage, here a new generation of photocage was designed employing the same *m*-NPA model but incorporated PDA as a more suitable Zn^{2+} chelator.

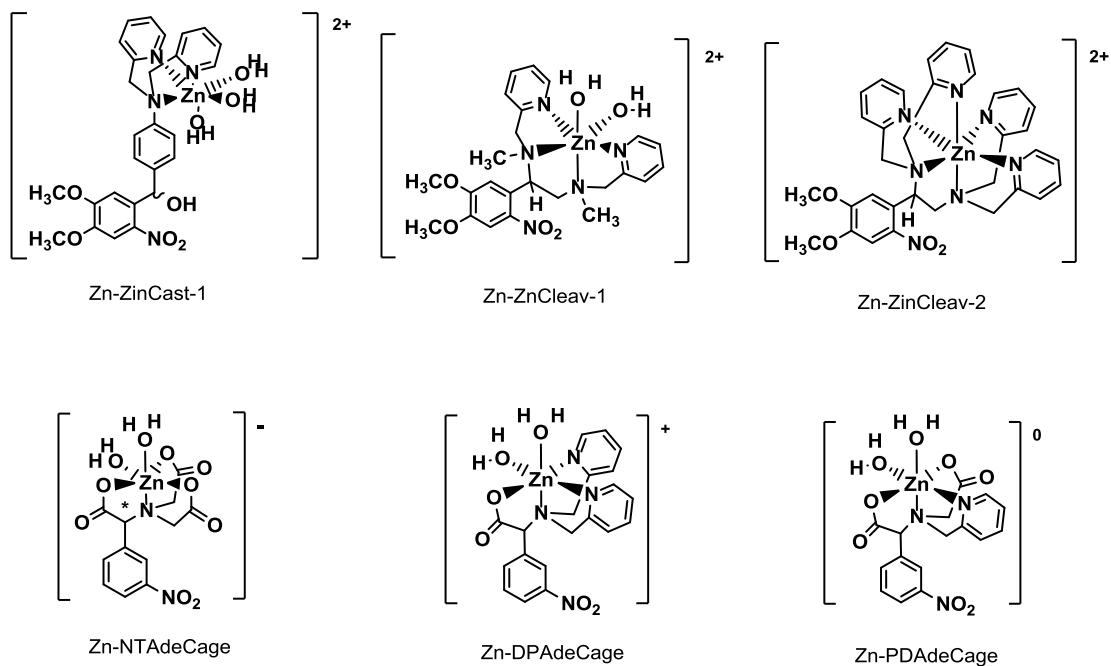


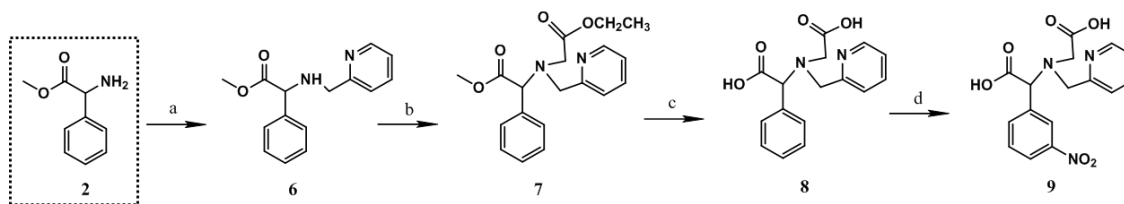
Fig 4.1 Zn²⁺ complexes with different charges.

4.2 Experimental Section

4.2.1 Materials and Methods

All reagents were purchased from Acros and Alfa Aesar at the highest commercial quality and used without further purification. Acetonitrile (CH₃CN) and dichloroethane (DCE) were dried before taking to use by a Seca Solvent Purification System. All chromatography and TLC were performed on either silica (230-400 mesh) from Silicycle or Aluminumoxide (basic, 50-200 μm, 60A) from Acros. TLCs were developed using mixtures of ether/hexanes, CH₂Cl₂/hexanes, ethyl acetate (EA)/hexanes and CH₂Cl₂/CH₃OH and were visualized with 254 or 365 nm light. ¹H and ¹³C NMR were obtained using a 500 MHz Bruker NMR instrument, the corresponding chemical shifts were reported in ppm on the δ scale relative to tetramethylsilane (TMS). IR spectra were recorded on a Bruker Vertex 70 FTIR and the samples were prepared as thin films on KBr plates or KBr pellets.

4.2.2 Synthetic Procedures



Scheme 4.1 Synthesis of DAPdeCage. Compound 2 was synthesized using the procedure described previously.

Methyl 2-((2-ethoxy-2-oxoethyl)(pyridin-2-ylmethyl)amino)-2-phenylacetate (7).

Compound **2** (1.64 g, 9.93 mmol) and 2-Pyridinecarboxaldehyde (945 μ L, 9.93 mmol) were combined in 1,2-dichloroethane (25 mL) in a 100 mL round bottomed flask and refluxed for 1 h. The mixture was allowed to cool down to room temperature. $\text{NaBH}(\text{OAc})_3$ (3.16 g, 14.9 mmol) was added and the resulting mixture was stirred for an additional 16 h. Water (20 mL) was added and the product was extracted into CH_2Cl_2 (3×10 mL). The organic layers were combined, dried over anhydrous Na_2SO_4 and filtered. The solvent was removed on a rotary evaporator to yield **6** as a bright yellow oil, which was used in the next step without further purification.

To a 250 mL round bottomed flask compound **6** (1.56 g, 6.09 mmol), ethyl bromoacetate (1015 μ L, 9.15 mmol), KI (101 mg, 0.609 mmol), K_2CO_3 (2.52 g, 18.27 mmol) were combined in acetonitrile (60 mL) and refluxed for 10 h. After the solvent was removed under reduced pressure, H_2O (40 mL) was added and the product was extracted into ethyl acetate (3×20 mL). The combined organic extracts were dried over anhydrous Na_2SO_4 , and the solvent was removed on a rotary evaporator. Flash chromatography on alumina (25:100, ethyl acetate:hexane) yielded **7** as a colorless oil (0.75 g, 36%). ^1H NMR δ 8.48 (d, $J = 4.9$ Hz, 1H), 7.75 (d, $J = 7.8$ Hz, 1H), 7.67 (td, $J = 7.6, 1.8$ Hz, 1H), 7.46 – 7.41 (m, 2H), 7.36 – 7.27 (m, 3H), 7.14 (ddd, $J = 7.3, 4.9, 1.2$ Hz, 1H), 8.48 (ddd, $J = 4.9, 1.7, 0.9$ Hz, 1H), 7.75 (d, $J = 7.8$ Hz, 1H), 7.67 (td, $J = 7.6, 1.8$ Hz, 1H), 7.46 – 7.41 (m, 2H), 7.36 – 7.27 (m, 3H), 7.14 (ddd, $J = 7.3, 4.9, 1.2$ Hz, 1H), 4.94 (s, 1H), 4.18 – 3.94 (m, 4H), 3.71 (s, 3H), 3.45 (dd, $J = 100.4, 17.8$ Hz, 2H), 1.19 (t, $J = 7.1$ Hz, 3H). ^{13}C NMR (CDCl_3) δ 172.7, 159.9, 149.1, 136.5, 136.2, 129.1, 128.6, 128.2, 123.1, 122.1, 67.6, 57.0, 51.8.

2-((Carboxymethyl)(pyridin-2-ylmethyl)amino)-2-phenylacetic acid (8). Compound **7** (614 mg, 1.79 mmol) was dissolved in CH₃OH (2 mL) in a 20 mL glass vial. NaOH (716 mg, 17.9 mmol) in 1 mL H₂O was carefully added using an ice bath. The mixture was stirred at room temperature for 18 h. After the reaction was completed, the solvent was removed and a small portion of H₂O was added. A small portion of H₂O was added and the aqueous pH was adjusted to 5. The product was extracted into ethyl acetate (3 × 15 mL). This procedure was repeated at pH 4 and the gathered organics were dried over anhydrous Na₂SO₄ and filtered. The solvent was removed under reduced pressure to give **8** as a white solid (91 mg, 17%). ¹H NMR (DMSO) δ 8.46 (d, *J* = 4.9 Hz, 1H), 7.78 (td, *J* = 7.7, 1.8 Hz, 1H), 7.56 (d, *J* = 7.8 Hz, 1H), 7.42 – 7.28 (m, 5H), 7.26 (ddd, *J* = 7.4, 4.9, 1.1 Hz, 1H), 4.74 (s, 1H), 3.97 – 3.86 (m, 2H), 3.30 (dd, *J* = 104.5, 17.9 Hz, 2H). ¹³C NMR (DMSO) δ 173.0, 172.5, 159.2, 148.4, 136.8, 128.6, 128.4, 128.0, 122.5, 122.2, 68.2, 56.8, 51.5.

2-((Carboxymethyl)(pyridin-2-ylmethyl)amino)-2-(3-nitrophenyl)acetic acid (DAPdeCage, 9). To a small vial compound **8** (64 mg, 0.21 mmol) was added in concentrated H₂SO₄ (2 mL) and stirred for 10 min. HNO₃ (70%, 200 μL) was added in one portion in the dark. The reaction was kept below 0 °C using a CH₃CN/dry ice bath. After 1.5 h, crushed ice was added to the mixture and the pH was adjusted to 4. The product was extracted into ethyl acetate (5 × 10 mL). The combined organics were dried over Na₂SO₄ and filtered. The solvent was removed on a rotary evaporator, giving **8** as a white solid (17 mg, 23%). ¹H NMR 8.47 (d, *J* = 4.0 Hz, 1H), 8.27 (s, 1H), 8.17 (d, *J* = 8.3 Hz, 1H), 7.88 (d, *J* = 7.7 Hz, 1H), 7.77 (t, *J* = 83 Hz, 1H), 7.66 (t, *J* = 8.0 Hz, 1H), 4.95 (s, 1H), 3.97 (s, 1H), 3.39 (s, 1H).

General Spectroscopic Methods

All solutions were prepared using spectroscopic grade solvents or Millipore (Biopak™ Ultrafiltration Cartridge) water. HEPES (4-(2-hydroxyethyl)-1-piperazineethanesulfonic acid), and KCl (99.8%) were bought from Fisher Scientific used without further purification. The pH values were recorded with Acumet pH glass electrode that was calibrated prior to use. Zn²⁺ stock solution was prepared from ZnCl₂ and standardized by titrating with terpyridine. DAPdeCage stock solution was prepared in CH₃OH before introducing to aqueous and the concentration was checked by UV each time prior to use. All the spectroscopic experiments

were performed and recorded at 25 °C. Absorption spectra were recorded on a Thermo Scientific Evolution 300 UV-vis spectrometer using Cary winUV software and the samples were placed on a 1.0 cm quartz cuvette. Fluorescence spectra were recorded on a Hitachi F-4500 spectrometer controlled by Pentium-IV PC run by FL solutions 2.0 software package. A 150 W Xe arc lamp (Ushio Inc.) operating at 5 A (current), 700 V was used for excitation and the samples were placed on a 1.0 cm quartz cuvette. LC-MS was carried on a Agilent Technologies 1200 series LC system and the traces at 254 nm was recorded for analysis. Ketoprofen (0.8 mM) was used as internal standard and all the samples were eluted with an isocratic mixture of 95:5 CH₃CN:H₂O containing 0.1% formic acid at a flow rate of 0.3 mL/min.

4.2.3 Determination of Zn²⁺ Binding Constants

A 2.0 mL of PAR (200 µM, HEPES pH 7.0) was prepared in a quartz cuvette and its UV spectrum was recorded. A 2.0 µL aliquot of ZnCl₂ (10 mM) was added and its spectrum was recorded. The solution was titrated with 4.0 µL increments of DAPdeCage (10 mM) and the corresponding spectra were recorded after each titration. To ensure reproducible results, the procedure was repeated in triplicate. The binding equilibrium is expressed as equation 1 and the binding constant (K') of the Zn(DAPdeCage) is calculated using equation 2, where $\beta'_{PAR} = 2.2 \times 10^{12} \text{ M}^{-1}$ and $\Delta\varepsilon_{500} = 6.6 \times 10^4$ ^[56].



$$\frac{[Zn(DAPdeCage)][PAR]^2}{[DAPdeCage][PAR_2Zn]} = \frac{K'}{\beta'_{PAR}} \quad (2)$$

$$[PAR_2Zn] = \frac{A_{500}}{\Delta\varepsilon_{500}} \quad (3)$$

$$[PAR] = [PAR]_{total} - 2[PAR_2Zn] \quad (4)$$

$$[Zn(DAPdeCage)] = [PAR_2Zn]_{initial} - [PAR_2Zn] \quad (5)$$

$$[DAPdeCage] = [DAPdeCage]_{total} - [Zn(DAPdeCage)] \quad (6)$$

K' was calculated at each data point, averaged and corrected for ligand protonation^[55]. The corrected binding constant was used to calculate the dissociation constant (K_d) of the Zn(DAPdeCage) complex.

The K_d of Zn(DAPdeCage) complex in HEPES/CH₃OH was measured in the same way by preparing 2.0 mL of PAR (200 μ M, HEPES pH 7.0 with 50% CH₃OH), adding 2.0 μ L of Zn²⁺ (10 mM) and 2.0 μ L increments of DAPdeCage (2 mM).

4.2.4 Quantum Efficiency

Calibration. A stock solution of 2.0 mM DAPdeCage (40 mM HEPES, 100 mM KCl, pH 7.5) was prepared and diluted to 1.5 mM, 1.0 mM and 0.5 mM. The LC traces of each sample were recorded. The area of the peak was determined by integration. The Zn(DAPdeCage) was calibrated in a same way.

Photolysis of DAPdeCage and Zn(DAPdeCage). A 2.5 mL solution of 2 mM DAPdeCage (HEPES, pH 7.5) was prepared in a quartz cuvette and irradiated at 365 nm for 15 s, 30 s, 45 s and 60 s separately. The LC traces of each solution were recorded and peak area was determined by integration. The concentration of DAPdeCage was calculated from the calibration curve and the corresponding quantum efficiency was calculated based on equation 7, where the intensity of the light source was determined as previously described. The quantum yield of Zn(DAPdeCage) was calibrated in a same way.

$$\text{Quantum Efficiency} = \frac{\Delta[\text{DAPdeCage}]/\text{Irradiation time}}{\text{Light Intensity}} \times N_A \quad (7)$$

4.2.5 Release of Caged Zn²⁺

A 2.0 mL of 10 μ M ZTRS solution (HEPES, pH 7.5) was prepared in a quartz cuvette and its emission spectrum was recorded. A 1 μ L aliquot of 20 mM ZnCl₂ was added to this cuvette and its spectrum was recorded. To another cuvette, a 2.0 mL solution containing 10 μ M ZTRS, 1 eq of Zn²⁺ and 3 eq of DAPdeCage was prepared and its spectrum was recorded.

The fluorescence changes upon zinc release was obtained by preparing a series of solutions each containing 2.0 mL of 10 μM Zn^{2+} with 3 eq of DAPdeCage and irradiating at 365 nm for 30 s, 60 s, 90 s...separately. After irradiation, a 10 μL aliquot of 2 mM ZTRS was added and the corresponding emission spectra were recorded.

The release of Zn^{2+} from Zn(DAPdeCage) in the presence of PAR followed the same procedure as described in **Section 3.2.5**.

4.2.6 Metal Selectivity

Ca-Zn exchange. A series of solutions (HEPES, pH 7.5) containing 20 μM DAPdeCage, 10 μM Zn^{2+} and 10 μM PAR was prepared. The solution was titrated with exponentially increased amounts of CaCl_2 from 1 eq to 512 eq and the UV spectrum was recorded.

4.3 Results and Discussion

4.3.1 Design and Synthesis

DAPdeCage was designed based on *N*-(2-Pyridylmethyl)iminodiacetic acid (PDA), a tetradentate chelator which also has a pM affinity for Zn^{2+} ^[55]. Compound **2** was synthesized using the esterification method described previously. Compound **6** was synthesized using a condensation reaction which formed an imine. The imine was then reduced by sodium triacetoxyhydroborate (STAB) to give **6** as the expected secondary amine. Since STAB is pretty sensitive to water, a few sieves was added before adding the salt to remove the water produced from the condensation reaction. The amine was further alkylated to give compound **7**. Hydrolysis of compound **7** yielded **8**, which had the desired PDA ligand cooperated to the aromatic scaffold. Like the synthesis of other *m*-NB based cages, the nitro group was introduced in the last step to avoid unnecessary handling and manipulation of photoactive compounds. It should be noted here that unlike the DPAdCage, which didn't suffer too much issue during synthesis, the last two steps in the synthesis of DAPdeCage were very wrenching. Both compound **7** and compound **8** have two carboxylic acid groups on its structure, which makes it rather hydrophilic compared to compound **4** and **5**. This feature takes advantage for

its application under a physiological condition but meanwhile means the product is hard to be extracted into organic phase in the absence of water. Several approaches, including adjust the pH to a variety of range from 1.5 (the pH at which PDA was obtained) to 6, or use different organic extracts were explored, yet the productivity was not improved significantly at these conditions due to its limited solubility in these organic solvents. Another approach that trying to obtain the product directly from aqueous did not work very well either, probably due to its small quantity in water.

4.3.2 Zn²⁺ Binding Studies

Similar to DPAdCage, the Zn(DAPdeCage) complex lacks spectroscopic signature therefore a competitive titration in the presence of 4-(2-Pyridyl-2-azo) resorcinol (PAR) was used to measure its binding affinity. By monitoring the absorbance changes at 500 nm where the PAR₂Zn forms, the binding constant (K') of Zn(DAPdeCage) was calculated using equation 2 while the relative components were calculated using equation 3-6. The volume changes upon DAPdeCage addition were adjusted to calculate the concentrations at each data set and the ligand protonation was also considered for correction^[55]. Under physiological condition, the Zn(DAPdeCage) has a measured K_d of 20.2 pM which is consistent with its structurally analog PDA ($K_d = 12.8 \text{ pM}$)^[55]. Since Zn²⁺ binds to 2-(aminoethyl)pyridine-*N*-monoacetic acid (AMPA) at 25.1 nM^[64], Zn(DAPdeCage) complex is suggested to have a ΔK_d of ~ 1000 .

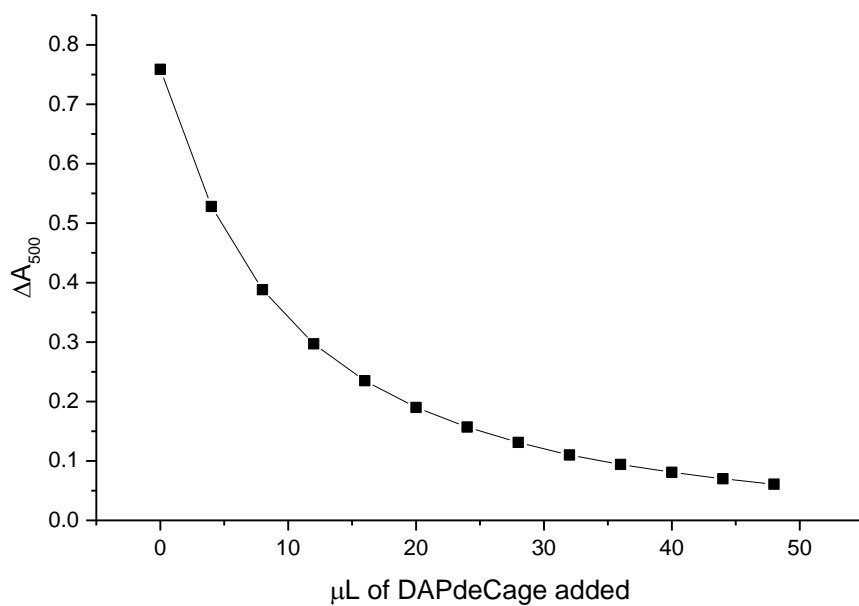
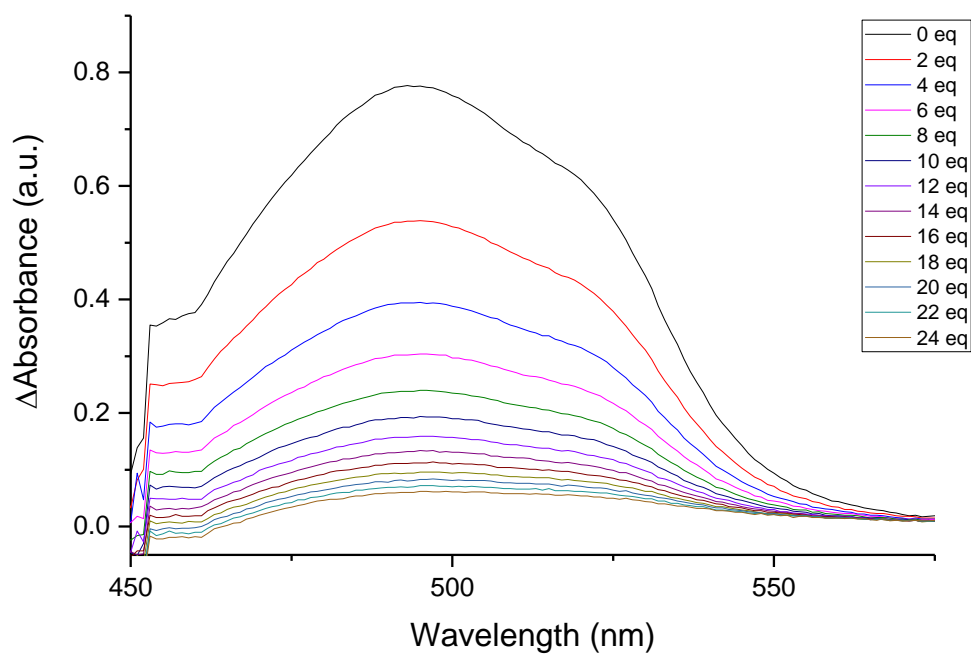
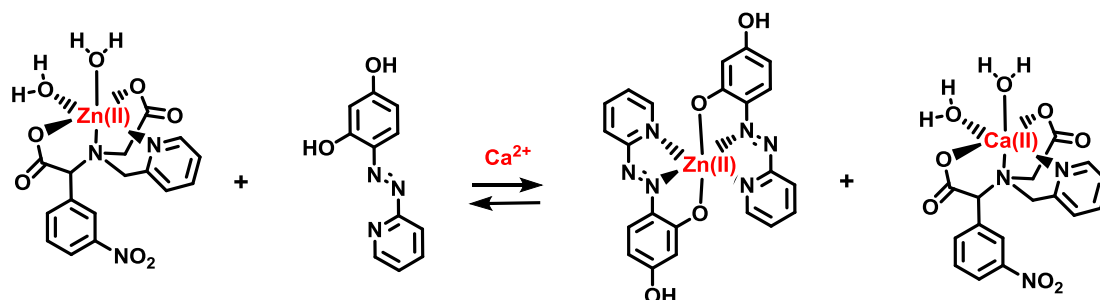


Fig 4.2 Competitive titration between DAPdeCage and PAR in the presence of Zn²⁺. A solution of 200 μM PAR and 10 μM Zn²⁺ (40 mM HEPES, 100 mM KCl, pH 7.0) was titrated against a stock solution of DAPdeCage (10 mM) and absorbance spectrum was recorded after each addition. The λ_{max} at 500 nm is attributed to the absorbance of PAR₂Zn. Adding DAPdeCage causes Zn²⁺ depletion from Zn-PAR complex and this is evidenced by a decreasing of the absorbance at 500 nm.

The DAPdeCage ligand has two carboxyl group and is electric neutral when binds Zn^{2+} . The Ca-Zn exchange study was carried out by titrating CaCl_2 solution to a mixture of $\text{Zn}(\text{DAPdeCage})$ and PAR (Fig 4.3, a). With an exponentially increased amount of Ca^{2+} , an absorbance enhancement at 500 nm together with a decrease at 412 nm was observed (Fig 4.3, b), indicating a substitution of Zn^{2+} by Ca^{2+} from $\text{Zn}(\text{DAPdeCage})$ complex when Ca^{2+} is prominently excess ($\sim\text{mM}$). Since typically the intracellular Ca^{2+} is kept at a level of ~ 100 nM and rises to ~ 10 μM in an signaling event^[47], we propose the influence of cellular Ca^{2+} on $\text{Zn}(\text{DAPdeCage})$ complex should be very limited.

a)



b)

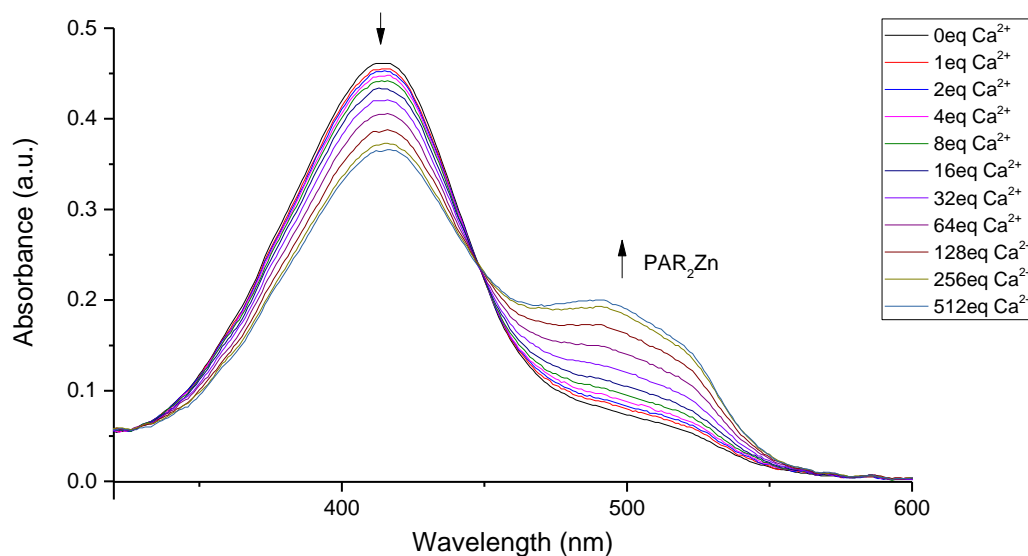


Fig 4.3. a) Ca-Zn exchange equilibrium. b) Ca-Zn exchange evidenced by PAR_2Zn formation. A series of solutions (HEPES, pH 7.5) containing 20 μM DAPdeCage, 10 μM Zn^{2+} and 10 μM PAR was prepared. The solution was titrated with exponentially increased amounts of CaCl_2 from 1 eq to 512 eq and the UV spectrum was recorded.

4.3.3 Photochemistry

The photochemistry of DAPdeCage was examined using the same method as described in section 2.3.3. By measuring the disappearance of DAPdeCage and $\text{Zn}(\text{DAPdeCage})$ on LC traces, the quantum efficiency of the apo cage and the metal complex were calculated to be 54% and 5.9% respectively. Further analysis of the m/z values indicated that *m*-Nitrobenzaldehyde (*m*-NB) and AMPA are major products of the photolysis (Fig 4.4, Fig 4.5, Scheme 4.2).

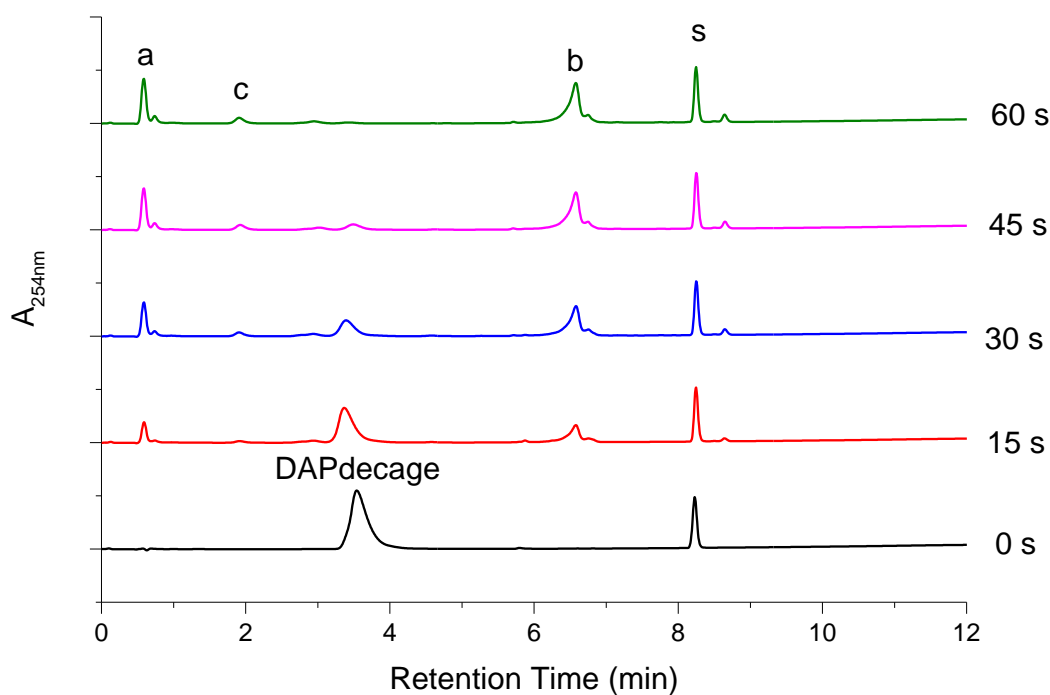


Fig 4.4. LC traces of DAPdeCage (2 mM, 40 mM HEPES, 100 mM KCl, pH 7.5) before and after irradiation at 365 nm. Ketoprofen (s) was used as internal standard. A disappearance of DAPdeCage accompanied with an appearance of major photoproducts (AMPA, a; *m*-nitrobenzaldehyde, b) and minor photoproducts was observed.

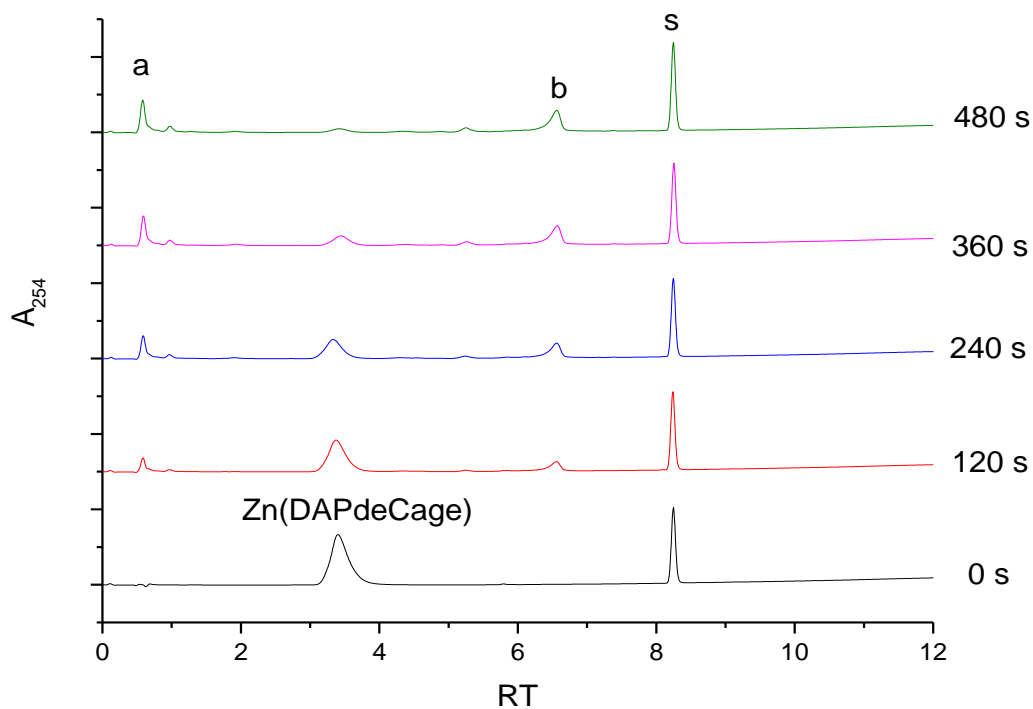
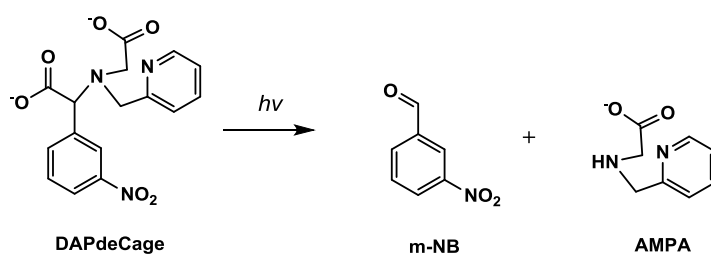


Fig 4.5. LC traces of Zn(DAPdeCage) (1 mM, 40 mM HEPES, 100 mM KCl, pH 7.5) before and after irradiation at 365 nm. Ketoprofen (s) was used as internal standard. A disappearance of Zn(DAPdeCage) accompanied with an appearance of major photoproducts (AMPA, a; *m*-nitrobenzaldehyde, b) were observed.

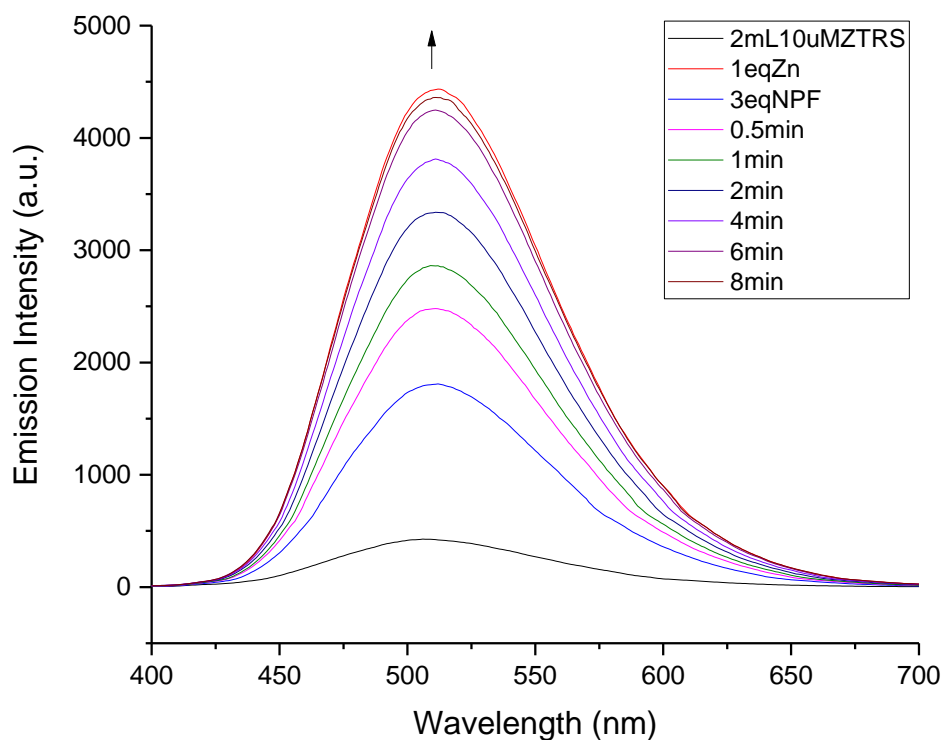


Scheme 4.2 Proposed DAPdeCage photolysis scheme. *m*-NB and AMPA are evidenced as two major photoproducts.

The release of caged Zn^{2+} was accessed by uncaging the complex in a quartz cuvette and monitor the released free Zn^{2+} using ZTRS ($K_d = 5.7$ nM). To avoid photo bleaching, the

samples without fluorescent sensor were irradiated for different seconds, and ZTRS was added to each sample after photolysis. Results showed that addition of 30 μM DAPdeCage to a solution of 10 μM $[\text{Zn}(\text{ZTRS})]^{2+}$ causes an immediate extinguish of fluorescence at 512 nm. Irradiating $\text{Zn}(\text{DAPdeCage})$ at 365 nm for about 5 min causes a restoration of the fluorescence, indicating the breakage of high affinity Zn^{2+} chelator PDA and a successful release of Zn^{2+} (Fig 4.6). The uncaging process was also monitored by PAR as previously described. As predicted, an absorption enhancement at 500 nm concomitant (Fig 4.7).

a)



b)

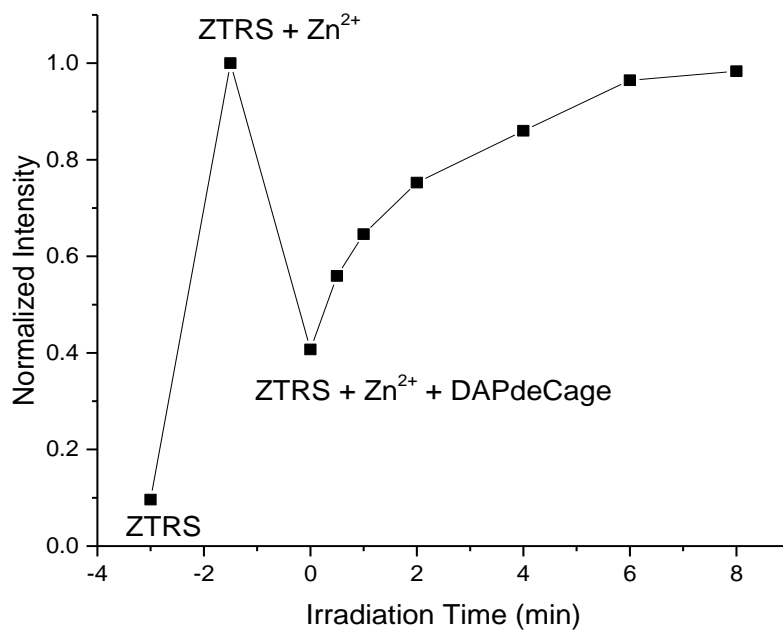


Fig 4.6. The Zn²⁺ released from Zn(DAPdeCage) was monitored by a fluorescent sensor, ZTRS. Emission Intensity of 10 μ M ZTRS was recorded before and after 10 μ M Zn²⁺ addition. Subsequent 30 μ M DPAdCage addition quenched the emission of Zn-ZTRS, while the followed irradiation led to a complete photolysis in ~ 8 min and restored the emission.

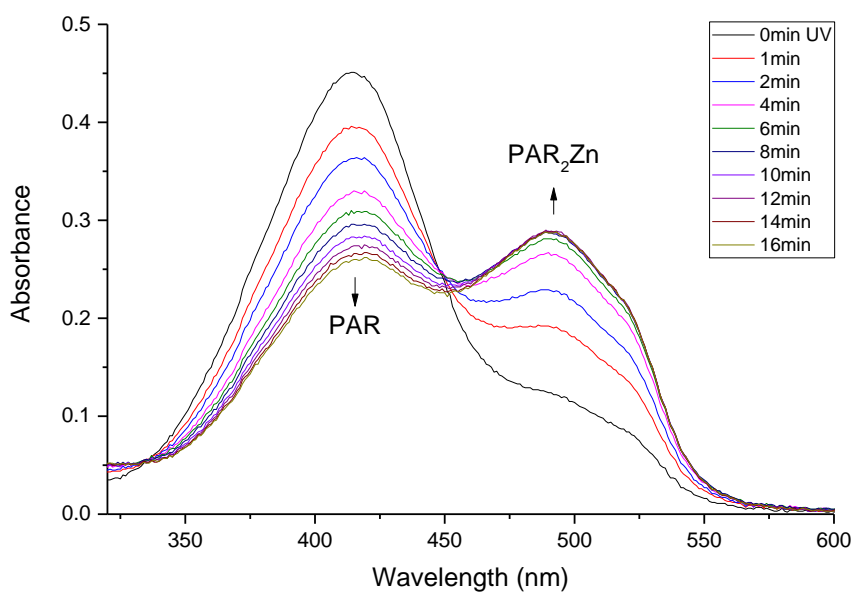


Fig 4.7. The Zn²⁺ released from Zn(DAPdeCage) was monitored by the formation of PAR₂Zn complex.

5 XDAPdeCage

5.1 Background

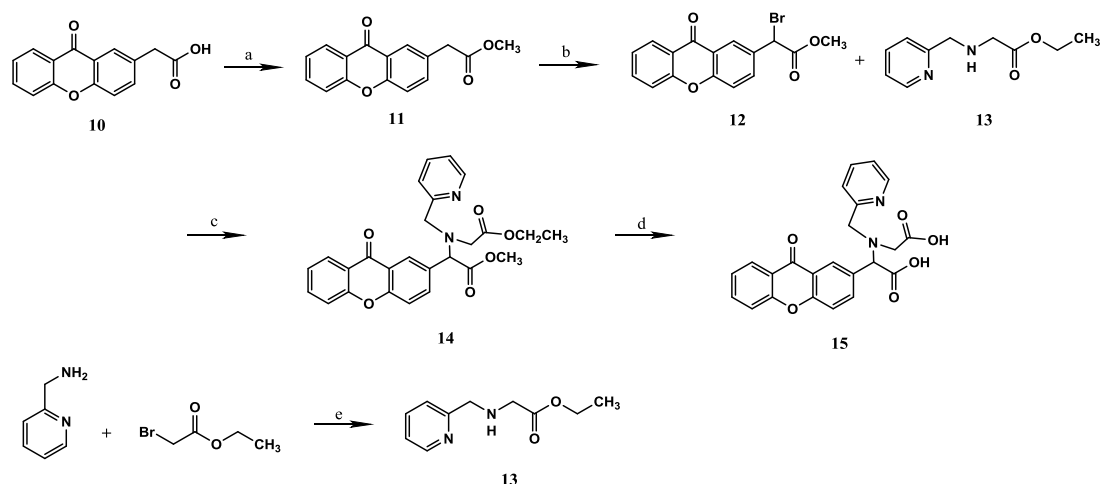
A recent study based on the singlet state photodecarboxylation of xanthone acetic acid has been reported, suggesting an efficient photoreaction to give carbanion intermediates^[65]. Both ketoprofen and xanthone are structurally similar to bezophenone chromophore, among which xanthone has a much better absorption at above 300 nm^{[65][66]}. In the design of the next generation of the photocages, we employed a xanthone based photoactive chromophore and integrated it with the PDA which is also the ligand for DAPdeCage. We expect this new XDAPdeCage would possess a better photo property than the previous reported photocages.

5.2 Experimental Section

5.2.1 Materials and Methods

All reagents were purchased from Acros and Alfa Aesar at the highest commercial quality and used without further purification. Acetonitrile (CH₃CN) and dichloroethane (DCE) were dried before taking to use by a Seca Solvent Purification System. All chromatography and TLC were performed on either silica (230-400 mesh) from Silicycle or Aluminumoxide (basic, 50-200 μm, 60A) from Acros. TLCs were developed using mixtures of ether/hexanes, CH₂Cl₂/hexanes, ethyl acetate (EA)/hexanes and CH₂Cl₂/CH₃OH and were visualized with 254 or 365 nm light. ¹H and ¹³C NMR were obtained using a 500 MHz Bruker NMR instrument, the corresponding chemical shifts were reported in ppm on the δ scale relative to tetramethylsilane (TMS). IR spectra were recorded on a Bruker Vertex 70 FTIR and the samples were prepared as thin films on KBr plates or KBr pellets.

5.2.2 Synthetic Procedure



Scheme 5.2 Synthesis of XDAPdeCage. Compound 10 was synthesized using a published method^[67].

Methyl 2-(9-oxo-9H-xanthene-2-yl)acetate (11). To a 250 mL round bottomed flask compound **10** (3.81 g, 15.0 mmol) was added in methanol (60 mL) and concentrated H₂SO₄ (10 mL) was added with stirring. The mixture was refluxed for 2.5 h. After the reaction was completed, the excess CH₃OH was removed and H₂O (50 mL) was added. The aqueous pH was adjusted to 8 using saturated Na₂CO₃ and extracted with ethyl acetate (3 × 30 mL). The combined organic layers were dried over anhydrous Na₂SO₄, filtered, and the solvent was removed under reduced pressure to give **11** as a white solid (2.60 g, 64.7%). ¹H-NMR δ 8.35 (dd, *J* = 8.0, 1.5 Hz, 1H), 8.25 – 8.20 (m, 1H), 7.73 (ddd, *J* = 8.7, 7.1, 1.7 Hz, 1H), 7.68 (dd, *J* = 8.6, 2.3 Hz, 1H), 7.53 – 7.46 (m, 2H), 7.39 (ddd, *J* = 8.1, 7.1, 1.0 Hz, 1H), 3.77 (s, 2H), 3.72 (s, 3H). ¹³C NMR (CDCl₃) δ 177.2, 171.7, 156.3, 155.5, 136.1, 135.0, 130.0, 127.2, 126.9, 124.1, 122.0, 121.8, 118.5, 118.1, 52.3, 40.5.

Methyl 2-bromo-2-(9-oxo-9H-xanthene-2-yl)acetate (12). To a 100 mL round bottomed flask compound **11** (1.69 g, 6.30 mmol), *N*-Bromosuccinimide (1.68 g, 9.45 mmol), 2,2'-Azobis(2-methylpropionitrile) (103 mg, 0.630 mmol) were mixed in 30 mL dichloroethane and stirred. The reaction was brought to reflux and stirred for 2.5 h. After the reaction completed, the solution was cooled down to room temperature and washed with H₂O (2 × 20 mL) and saturated NaCl (20 mL). The organic layer was dried over anhydrous Na₂SO₄ and filtered. The solvent was removed on a rotary evaporator to give a brown solid. Flash chromatography on silica (2:1, ether:hexane) yielded **11** as a white solid (1.26 g, 57.6%). ¹H-NMR (CDCl₃) δ 8.39 (d, *J* = 2.4 Hz, 1H), 8.34 (dd, *J* = 8.0, 1.6 Hz, 1H), 8.06 (dd, *J* = 8.8,

2.4 Hz, 1H), 7.75 (ddd, $J = 8.6, 7.1, 1.7$ Hz, 1H), 7.58 – 7.49 (m, 2H), 7.41 (ddd, $J = 8.0, 7.2, 1.0$ Hz, 1H), 5.50 (s, 1H), 3.82 (s, 3H). ^{13}C NMR (CDCl_3) δ 176.7, 168.7, 156.5, 156.2, 135.5, 135.3, 131.8, 126.9, 124.5, 121.9, 126.9, 124.5, 121.9, 121.6, 119.3, 118.2, 53.7, 45.2.

Ethyl (pyridin-2-ylmethyl)glycinate (13). 2-Picolylamine (1.1 g, 10 mmol), ethyl bromoacetate (1.1 mL, 10 mmol), NaI (0.15 g, 1.0 mmol) and K_2CO_3 (4.1 g, 30 mmol) were combined in 50 mL of acetonitrile. The mixture was refluxed for 8 h. The solvent was removed then H_2O (40 mL) was added and the product was extracted into ethyl acetate (3×20 mL). The organic extracts were combined and dried over anhydrous Na_2SO_4 . The solvent was removed under reduced pressure to give a yellow oil. Flash chromatography on alumina (1:1 ethyl acetate/hexane \rightarrow ethyl acetate) yielded **13** (1.01 g, 52%) as a bright colorless oil. ^1H NMR (CDCl_3): δ 8.55 (ddd, $J = 4.9, 1.7, 0.9$ Hz, 1H), 7.64 (td, $J = 7.7, 1.8$ Hz, 1H), 7.32 (d, $J = 7.8$ Hz, 1H), 7.20 – 7.11 (m, 1H), 4.18 (q, $J = 7.1$ Hz, 2H), 3.94 (s, 2H), 3.46 (s, 2H), 1.26 (t, $J = 7.1$ Hz, 4H). ^{13}C NMR (CDCl_3) δ 172.2, 159.2, 149.4, 136.5, 122.2, 122.1, 60.8, 54.6, 50.5, 14.3.

2-((2-Ethoxy-2-oxoethyl)(pyridin-2-ylmethyl)amino)-2-(9-oxo-9H-xanthen-2-yl)acetate (14). Compound **12** (780 mg, 2.25 mmol), compound **13** (436 mg, 2.25 mmol), NaI (34 mg, 0.23 mmol) and K_2CO_3 (931 g, 6.75 mmol) were combined in acetonitrile (30 mL). After refluxing for 8 h, the solvent was removed under reduced pressure. H_2O (40 mL) was added and the product was extracted into ethyl acetate (3×20 mL) and washed with saturated NaCl. The combined organics were dried over anhydrous Na_2SO_4 , filtered, and the solvent was removed under reduced pressure to give a yellow oil. . Flash chromatography on alumina (1:1 \rightarrow 2:1 ethyl acetate/hexane) yielded **14** as a colorless oil (497 mg, 48%). ^1H NMR (CDCl_3): δ 8.49 (ddd, $J = 4.9, 1.7, 1.0$ Hz, 1H), 8.36 – 8.29 (m, 2H), 7.96 (dd, $J = 8.8, 2.2$ Hz, 1H), 7.79 – 7.65 (m, 3H), 7.55 – 7.45 (m, 2H), 7.39 (ddd, $J = 8.0, 7.1, 1.0$ Hz, 1H), 7.15 (ddd, $J = 6.6, 4.9, 1.4$ Hz, 1H), 5.07 (s, 1H), 4.29 – 3.96 (m, 4H), 3.77 (s, 3H), 3.49 (dd, $J = 114.0, 17.8$ Hz, 2H), 1.21 (t, $J = 7.1$ Hz, 3H). ^{13}C NMR (CDCl_3) δ 176.9, 172.1, 171.3, 159.3, 156.2, 149.0, 136.8, 135.6, 135.1, 132.5, 126.9, 124.2, 123.2, 122.3, 121.2, 121.7, 118.8, 67.8, 60.7, 57.8, 52.2, 51.6.

2-((Carboxymethyl)(pyridin-2-ylmethyl)amino)-2-(9-oxo-9H-xanthen-2-yl)acetic acid (XDAPdeCage, 15). Compound **14** (250 mg, 0.54 mmol) was dissolved in CH₃OH (2 mL). NaOH (304 mg, 7.6 mmol) in 700 μ L H₂O was carefully added. The resulting mixture was stirred at 23 °C overnight. After the reaction completed, the excess CH₃OH was removed and a small portion of water was added. The aqueous pH was adjusted to 4. Removing solvent gives **15** as a white solid (46 mg, 20.3%). ¹H NMR (DMSO): δ 8.48 (d, *J* = 4.4 Hz, 1H), 8.22 – 8.16 (m, 2H), 7.94 (dd, *J* = 8.7, 2.2 Hz, 1H), 7.91 – 7.86 (m, 1H), 7.82 (t, *J* = 7.3 Hz, 1H), 7.68 (dd, *J* = 8.5, 3.4 Hz, 2H), 7.58 (d, *J* = 7.8 Hz, 1H), 7.49 (t, *J* = 7.2 Hz, 1H), 7.31 – 7.26 (m, 1H), 4.96 (s, 1H), 4.00 (s, 2H), 3.40 (dd, *J* = 100, 17.9 Hz, 2H).

General Spectroscopic Methods

All solutions were prepared using spectroscopic grade solvents or Millipore (BiopakTM Ultrafiltration Cartridge) water. HEPES (4-(2-hydroxyethyl)-1-piperazineethanesulfonic acid), and KCl (99.8%) were bought from Fisher Scientific used without further purification. The pH values were recorded with Acumet pH glass electrode that was calibrated prior to use. Zn²⁺ stock solution was prepared from ZnCl₂ and standardized by titrating with terpyridine. XDAPdeCage was stocked in its solid form and prepared freshly in CH₃OH/H₂O (with 5 drops of NaOH to ensure its solubility). All the spectroscopic experiments were performed and recorded at 25 °C. Absorption spectra were recorded on a Thermo Scientific Evolution 300 UV-vis spectrometer using Cary winUV software and the samples were placed on a 1.0 cm quartz cuvette. Fluorescence spectra were recorded on a Hitachi F-4500 spectrometer controlled by Pentium-IV PC run by FL solutions 2.0 software package. A 150 W Xe arc lamp (Ushio Inc.) operating at 5 A (current), 700 V was used for excitation and the samples were placed on a 1.0 cm quartz cuvette. LC-MS was carried on a Agilent Technologies 1200 series LC system and the traces at 254 nm was recorded for analysis. Isonicotinic acid (4.84 mM) was used as internal standard and all the samples were eluted with an isocratic mixture of 95:5 CH₃CN:H₂O containing 0.1% formic acid at a flow rate of 0.3 mL/min.

5.2.3 Determination of Zn²⁺ Binding Constants

A 2.0 mL of PAR (200 μ M, HEPES pH 7.0) was prepared in a quartz cuvette and its UV spectrum was recorded. A 2.0 μ L aliquot of ZnCl₂ (10 mM) was added and its spectrum was recorded. The solution was titrated with 4.0 μ L increments of XDAPdeCage (4 mM) and the corresponding spectra were recorded after each addition. The procedure was repeated in triplicate and binding constant (K') of the Zn(XDAPdeCage) was calculated using equation 2.



$$\frac{[Zn(DAPdeCage)][PAR]^2}{[DAPdeCage][PAR_2Zn]} = \frac{K'}{\beta'_{PAR}} \quad (2)$$

$$[PAR_2Zn] = \frac{A_{500}}{\Delta\varepsilon_{500}} \quad (3)$$

$$[PAR] = [PAR]_{total} - 2[PAR_2Zn] \quad (4)$$

$$[Zn(DAPdeCage)] = [PAR_2Zn]_{initial} - [PAR_2Zn] \quad (5)$$

$$[DAPdeCage] = [DAPdeCage]_{total} - [Zn(DAPdeCage)] \quad (6)$$

K' was calculated at each data point, averaged and corrected for ligand protonation^[55]. The corrected binding constant was used to calculate the dissociation constant (K_d) of the Zn(XDAPdeCage) complex.

The K_d of Zn(XDAPdeCage) complex in HEPES/CH₃OH was measured in the same way by preparing 2.0 mL of PAR (200 μ M, HEPES pH 7.0 with 50% CH₃OH), adding 2.0 μ L of Zn²⁺ (10 mM) and 1.5 μ L increments of XDAPdeCage (4 mM).

5.2.4 Quantum Yield of Photolysis

Calibration. A stock solution of 1.0 mM of XDAPdeCage (40 mM HEPES, 100 mM KCl, pH 7.5, 50% (v/v) CH₃OH) was prepared and diluted to 500 μ M, 250 μ M and 125 μ M. The samples were injected into LC-MS and the UV traces of each solution were recorded. The area of the peak was determined by integration. The Zn(XDAPdeCage) was calibrated in the same way.

Photolysis of XDAPdeCage and [Zn(XDAPdeCage)]. A 2.5 mL solution of 1.5 mM XDAPdeCage (40 mM HEPES, 100 mM KCl, pH 7.5, 50% (v/v) CH₃OH) was prepared in a

quartz cuvette and irradiated with a LED UV light (365 nm, 3 W) for 15 s, 30 s, 45 s, 60 s separately. The LC traces of each solution were recorded and the area of the XDAPdeCage peak was determined by integration. The concentration of XDAPdeCage was calculated from the calibration curve and the corresponding quantum efficiency was calculated from equation 7, where the intensity of the light source was determined as previously described. The quantum yield of Zn(XDAPdeCage) was calibrated in a same way.

$$\text{Quantum Efficiency} = \frac{\Delta[\text{XDAPdeCage}]/\text{Irradiation time}}{\text{Light Intensity}} \times N_A \quad (7)$$

This experiment was also repeated by preparing XDAPdeCage and Zn(XDAPdeCage) in a H₂O (pH 7.5)/CH₃OH mixture.

5.2.5 Release of Caged Zn²⁺

The emission spectra of 10 μM ZTRS and 10 μM Zn(ZTRS)²⁺ were recorded as previously described. To another cuvette, a 2.0 mL solution containing 10 μM ZTRS, 1 eq of Zn²⁺ and 3 eq of XDAPdeCage was prepared and its spectrum was recorded. The changes in emission spectra upon zinc release was recorded by preparing a series of solutions each containing 2.0 mL of 10 μM Zn²⁺ and 3 eq of XDAPdeCage and irradiating at 365 nm for 15 s, 30 s, 45 s...separately. A 10 μL aliquot of 2 mM ZTRS was added to each of the resulting solution and the corresponding spectra was recorded.

The release of Zn²⁺ from Zn(XDAPdeCage) in the presence of PAR was monitored as described in **Section 2.2.5**.

5.3 Results and Discussion

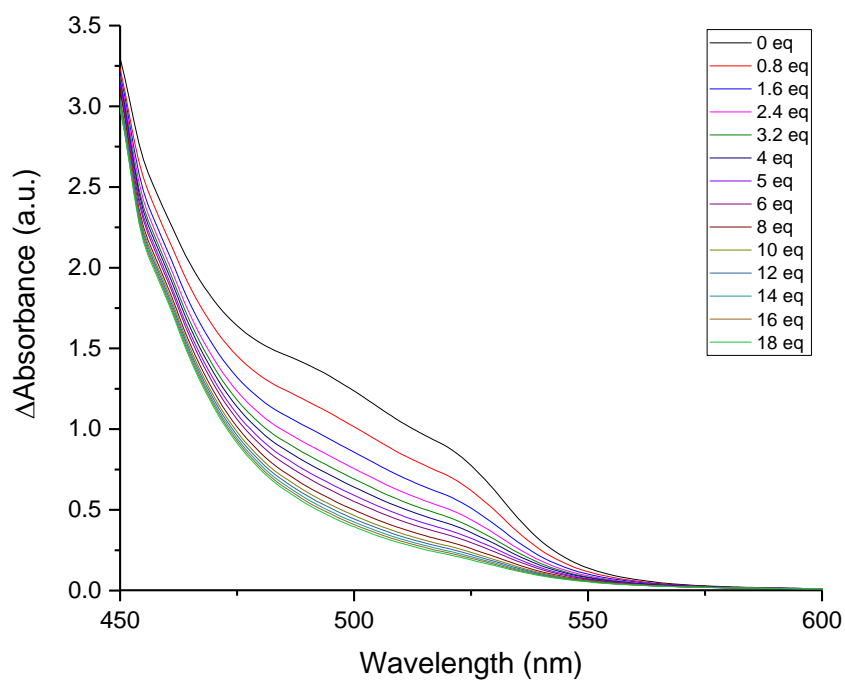
5.3.1 Design and Synthesis

XDAPdeCage was designed based on DAPdeCage but replaced the benzyl group with xanthone. Compound **10** was synthesized using a literature described method involving Ulmann coupling^[67]. Compound **12** was synthesized using Wohl-Ziegler bromination. The ligand STAB was synthesized separately and incorporated to the xanthone scaffold, followed by a saponification that gives XDAPdeCage as the final product. While DAPdeCage suffered from some issue that hard to be extracted from water, adjusting pH to 4 after hydrolysis led to a precipitation of white solid which was proved to be XDAPdeCage by both NMR and LC-MS. This may be attributed to the less polarity of the XDAPdeCage compared to DAPdeCage. On the other hand, XDAPdeCage is not as soluble as DAPdeCage in methonal or H₂O. To ensure the compound is fully dissolved in these solvents for characterization, an approximately 0.9 eq of base (NaOH) was added to deprotonate the protons.

5.3.2 Zn²⁺ Binding Studies

The binding property of XDAPdeCage was quantified by competitive titration between PAR₂Zn complex and the cage as previously described. Formation of the new Zn(XDAPdeCage) complex was indirectly evidenced by a decreasing PAR₂Zn absorbance at 500 nm. The experiment was repeated in triplicate and the averaged equilibrium constant K_d was calculated to be 9.2 ± 0.4 pM, which is close to the K_d of DAPdeCage (20.2 pM) and the reported K_d of PDA ligand (12.8 pM)^[64]. Like the *m*-NB derived DAPdeCage, XDAPdeCage also has a moderate ΔK_d of >1000 to release Zn²⁺.

a)



b)

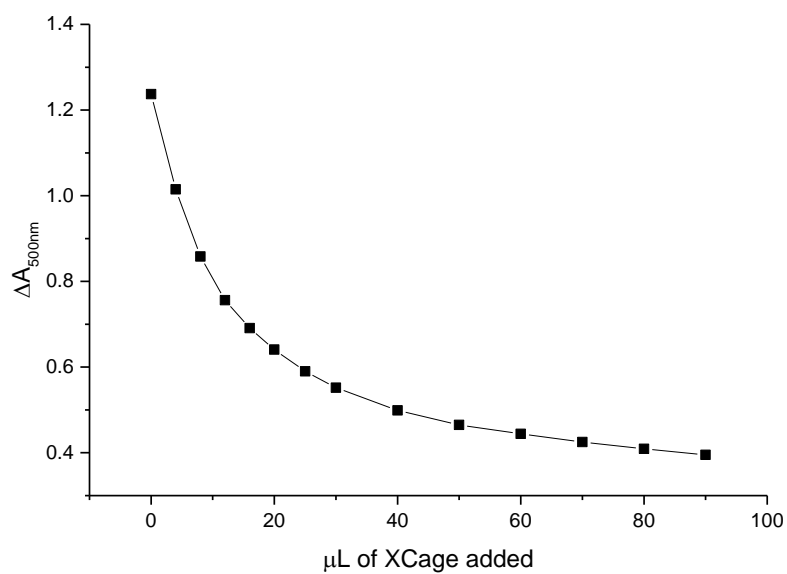


Fig 5.1 Competitive titration between PAR_2Zn and XDAPdeCage. A solution of 200 μM PAR and 10 μM Zn^{2+} (40 mM HEPES, 100 mM KCl, pH 7.0) was titrated against a stock solution of XDAPdeCage (4 mM) and absorbance spectrum was recorded after each addition. The λ_{max} at 500 nm is attributed to

the absorbance of PAR_2Zn . Adding XDAPdeCage causes Zn^{2+} depletion from PAR_2Zn and this is evidenced by a decreasing of the absorbance at 500 nm.

The metal exchange study of XDAPdeCage was performed in the same condition as DAPdeCage (Fig 5.2). Since the two cages are structurally analog and have similar binding affinities, it is not surprising we got a very close result which suggests the substitution of Zn^{2+} by Ca^{2+} can only happen when Ca^{2+} is at $\sim\text{mM}$ range. At typically physiological conditions, the influence of cellular Ca^{2+} on $\text{Zn}(\text{DAPdeCage})$ complex is not supposed to be a huge concern.

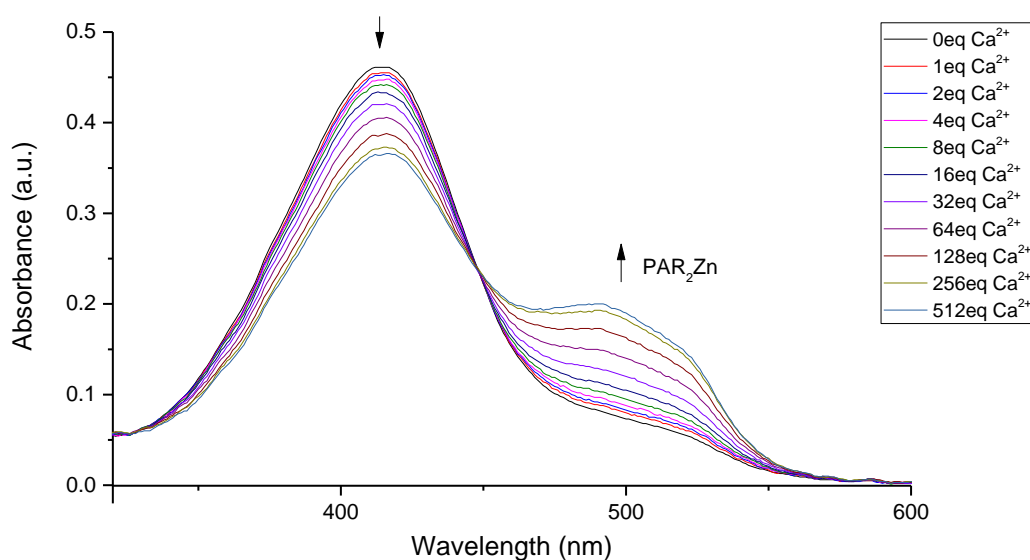
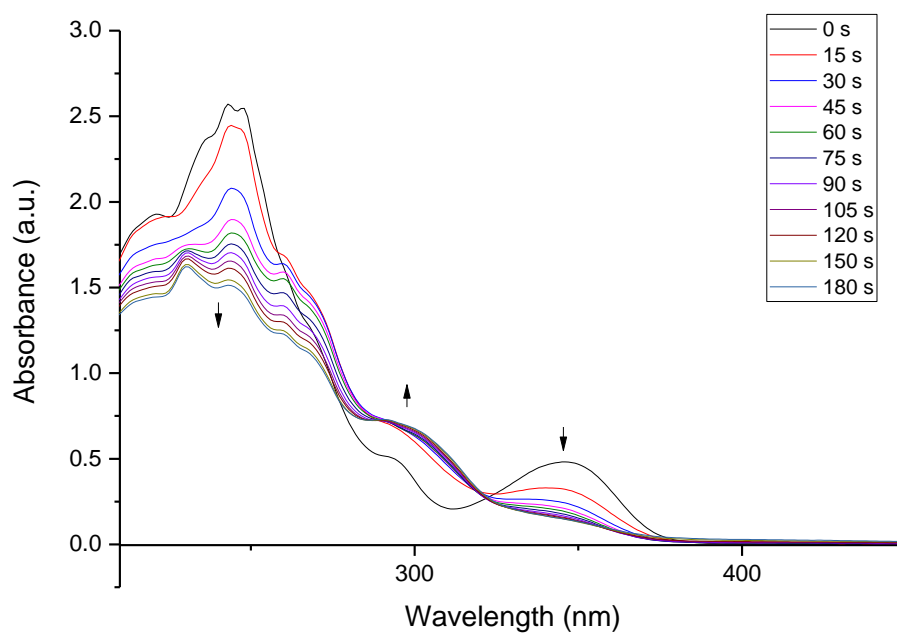


Fig 5.2. Ca-Zn exchange evidenced by PAR_2Zn formation. A series of solutions (HEPES, pH 7.5) containing 20 μM XDAPdeCage, 10 μM Zn^{2+} and 10 μM PAR was prepared. The solution was titrated with exponentially increased amounts of CaCl_2 from 1 eq to 512 eq and the UV spectrum was recorded.

5.3.3 Photochemistry

To determine the quantum yield of XDAPdeCage, the LC-MS spectra of the compound before and after photolysis was analyzed. The sample was initially prepared in HEPES buffer (40 mM HEPES, 100 mM KCl, pH 7.5), however, after irradiating 1 mM XDAPdeCage for 60 s, the transparent solution turned to an opaque suspension. Repeated experiments using 10% and 20% CH₃OH as co-solvent or replacing HEPES with H₂O led to the same results. This may be attributed to the limited solubility of photoproducts in these aqueous. To avoid the potential light scattering and also to analyze the corresponding products, a solution of 1.5 mM XDAPdeCage was prepared in 1:1 (v/v) HEPES/CH₃OH and irradiated for up to 60 s. A complete photolysis of the XDAPdeCage within 1 min was evidenced from the LC traces obtained (Fig 5.7). To propose the products of this photoreaction, a control study was conducted by irradiating the cage in the absence of buffer (1:1 H₂O/CH₃OH). By comparing the retention time as well as the m/z values, it is hypothesized that upon light irradiation, XDAPdeCage goes a photo-decarboxylation with a synchronous formation of xanthone-derived secondary amine (Fig 5.4, compound a). A second reaction pathway may involve a formation of an unstable imine which was further decomposed into a xanthone based aldehyde (Fig 5.4, compound b) as well as other minor possible photoproducts (Fig 5.4, compound c and d). The quantum yield of XDAPdeCage photolysis in HEPES/CH₃OH was calculated to be 17%. The photoactivity of Zn(XDAPdeCage) in HEPES/CH₃OH was also examined using the same method and the quantum yield of the complex was determined to be 13% (Fig 5.5, Fig 5.8).

a)



b)

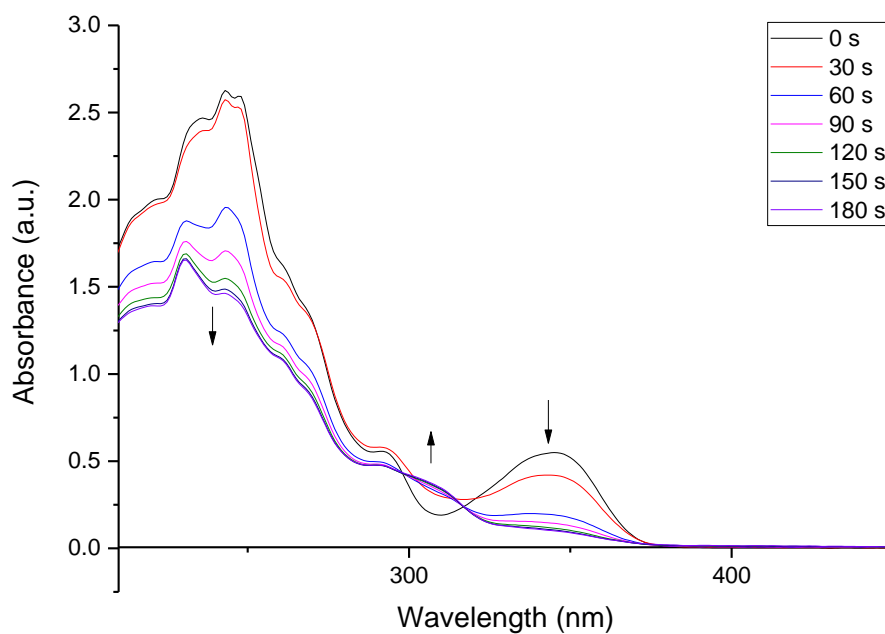


Fig 5.3. a) Absorbance changes of 100 μM apo-XDAPdeCage (40 mM, HEPES, 100 mM KCl, pH 7.5) upon irradiation. b) Absorbance changes of 100 μM Zn-XDAPdeCage complex (40 mM, HEPES, 100 mM KCl, pH 7.5) upon irradiation.

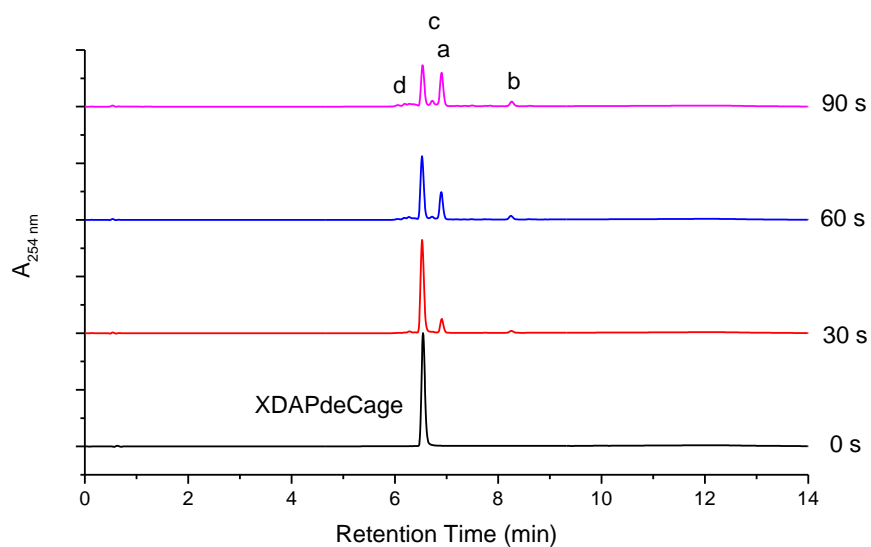


Fig 5.4. LC traces of XDAPdeCage (1 mM, H₂O pH 7.5 with 50% CH₃OH as cosolvent) before and after photolysis. Isonicotinic acid (4.84 mM) was used as internal standard

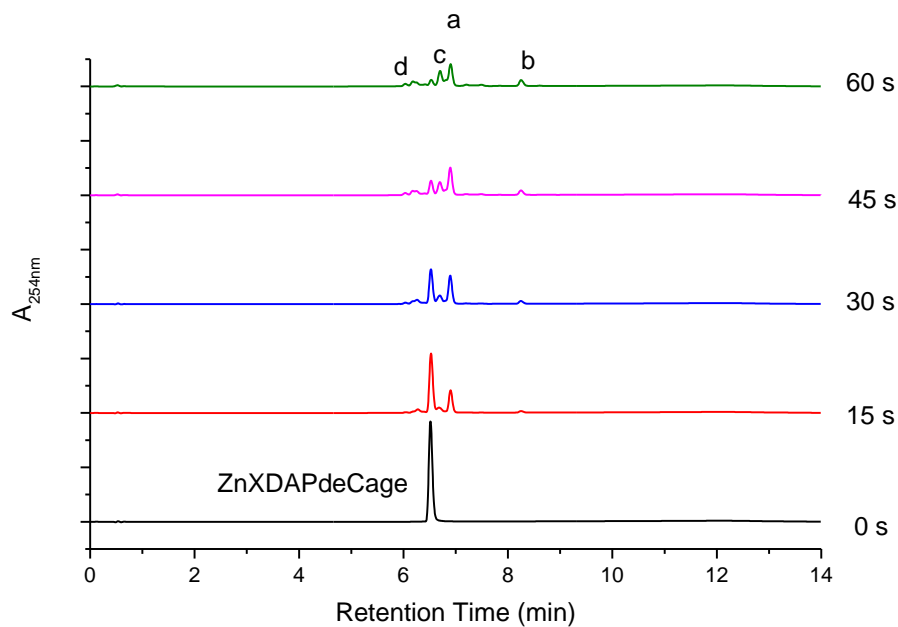


Fig 5.5. LC traces of Zn(XDAPdeCage) (1 mM, H₂O pH 7.5 with 50% CH₃OH as cosolvent) before and after photolysis. Isonicotinic acid (4.84 mM) was used as internal standard

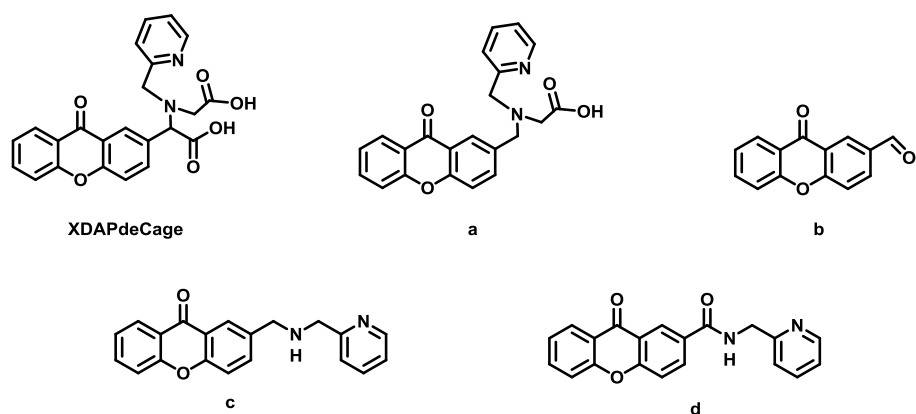


Fig 5.6 Proposed photoproducts upon XDAPdeCage uncaging, evidenced from LC-MS.

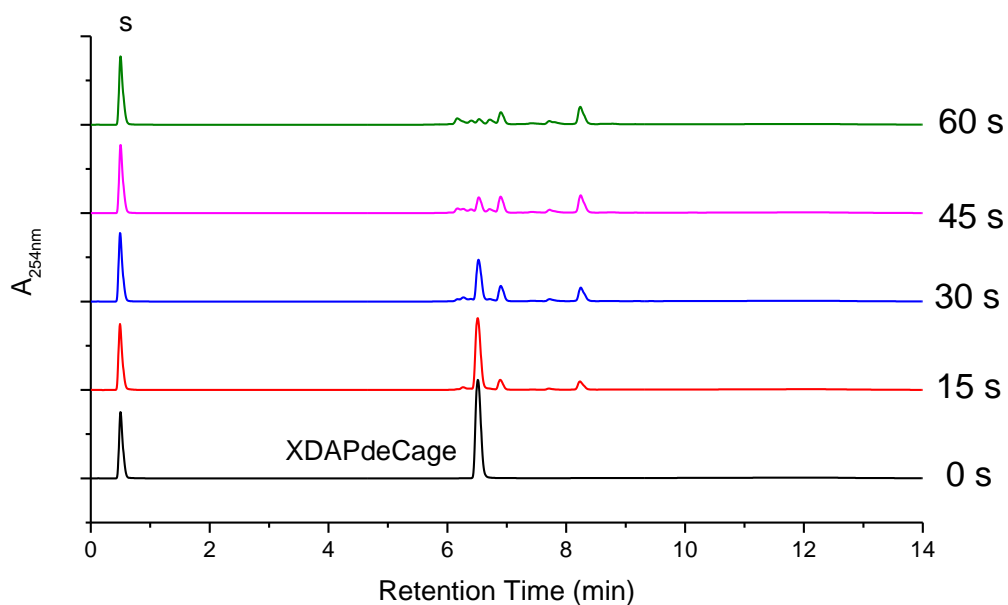


Fig 5.7. LC traces of XDAPdeCage (1.5 mM, HEPES pH 7.5 with 50% CH₃OH as cosolvent) before and after photolysis.

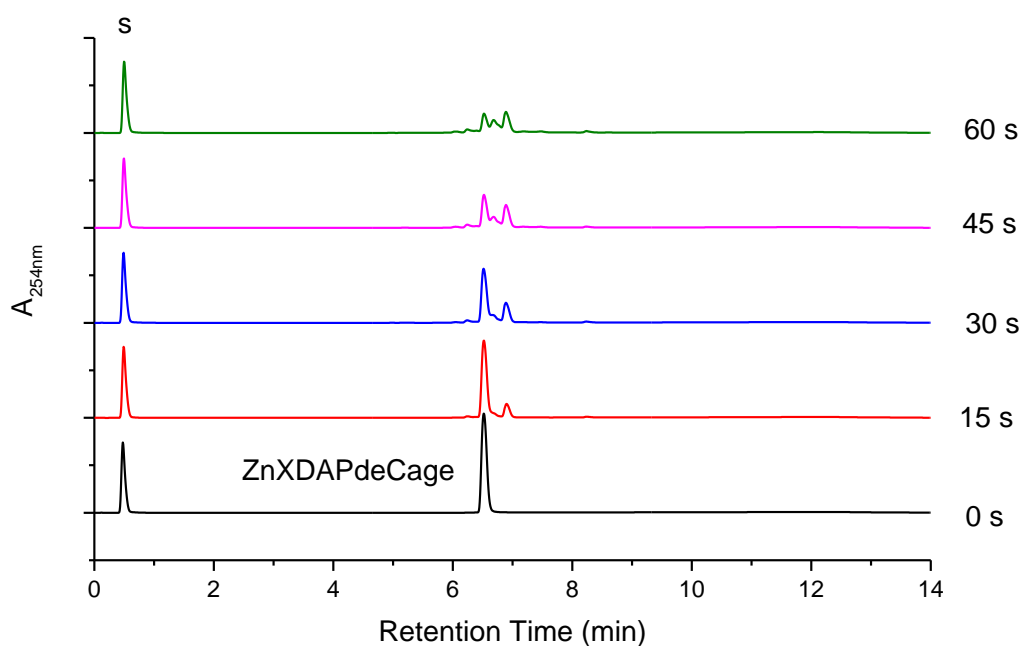
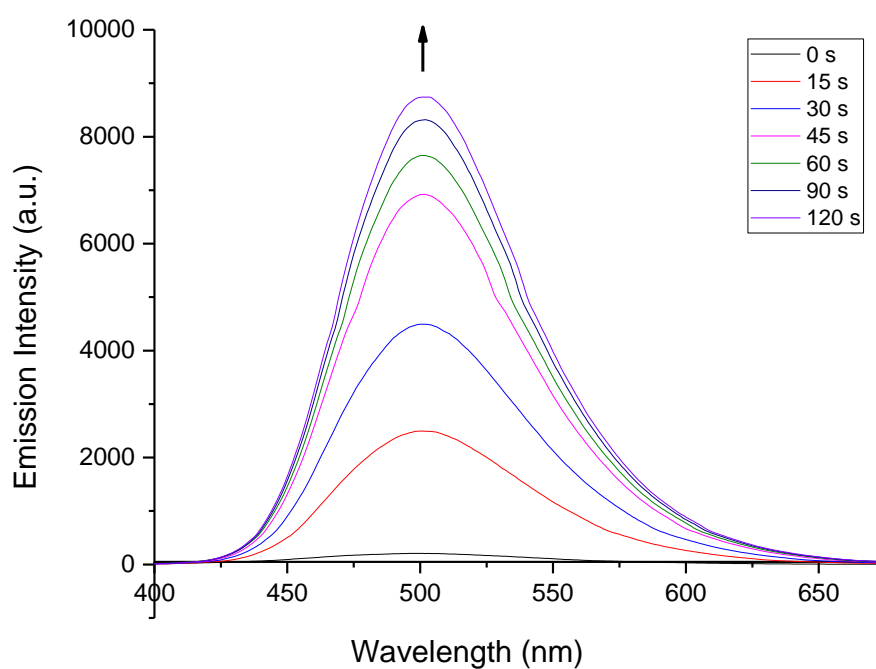


Fig 5.8. LC traces of Zn(XDAPdeCage) (1.5 mM, HEPES pH 7.5 with 50% CH₃OH as cosolvent) before and after photolysis.

The uncaging of Zn²⁺ was further analyzed using ZTRS ($K_d = 5.7$ nM). Addition of 30 μ M XDAPdeCage to a solution of 10 μ M [Zn(ZTRS)]²⁺ (1:1 HEPES/ACN) causes an immediate extinguish of fluorescence at 512 nm. Irradiating [Zn(XDPAdeCage)]⁺ at 365 nm causes a restoration of the fluorescence within 3 min, indicating the breakage of high affinity Zn²⁺ chelator XDPAdeCage and a successful release of free Zn²⁺ (Fig 5.9).

a)



b)

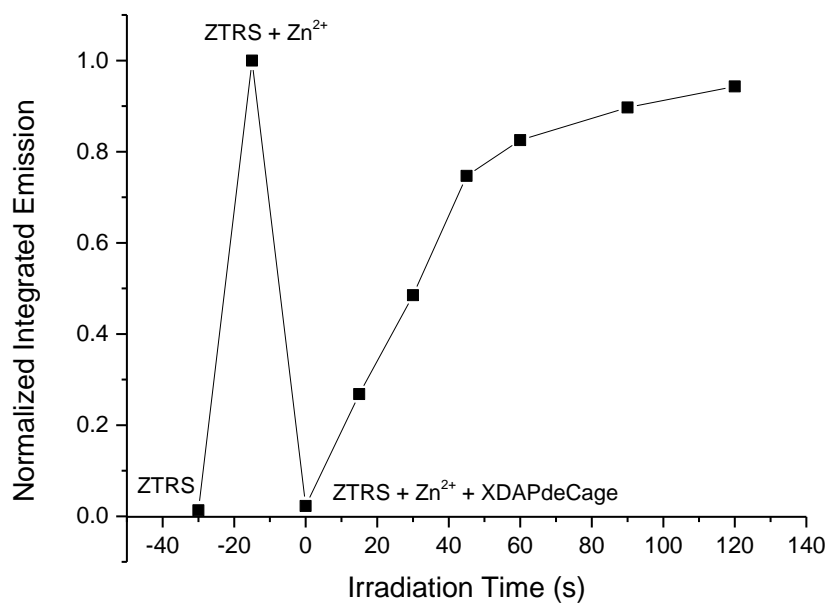


Fig 5.9. a,b) Uncaging Zn²⁺ monitored by fluorescent sensor ZTRS. Emission Intensity of 10 μ M ZTRS was recorded before and after 10 μ M Zn²⁺ addition. Subsequent 30 μ M XDAPdeCage addition quenched the emission of Zn-ZTRS, while the followed irradiation led to a complete photolysis in \sim 2 min and restored the emission.

6 Summary and Conclusion

The evidence of zinc as signaling molecule and further proofs of its role as first/second messenger in cell communication distinguishes zinc from the other transition metals in the body and gives it a unique position in bioinorganic chemistry. Upon stimulation, a large pool of zinc can be released from its binding sites and triggers signaling event. The transiently increased zinc is mainly driven by two mechanisms^[68]. One involves zinc efflux from vesicles or “zincosomes” and is mediated by membrane transport proteins. The other involves the changes in cellular redox potential and is mediated by cytosolic proteins. To artificially introduce Zn^{2+} into a biological system, one current strategy is to exogenously buffer the cells with Zn^{2+} salt. While this is the most widely used method by far, it risks overwhelming the system with excess Zn^{2+} that may cause unfavorable physiological responses.

Photocages provide an alternative way to stimulate Zn^{2+} signaling. By varying the intensity, area and duration of the irradiation, Zn^{2+} fluctuations can be controlled quantitatively, spatially as well as temporally. The earlier work of our group members attributes to the development of a number of Zn^{2+} cages including *Cast*, *Cleav*, and NTAdCage. Among them, the *Cast* and *Cleav* series utilize the classical *o*-nitrobenzyl photoreaction which intramolecular hydrogen abstraction by the excited nitro group leads to the formation of the *aci*-nitro intermediate, while the NTAdCage is dependent on the light-induced photodecarboxylation of *m*-nitrophenylacetate. The decarboxylation reaction is carbanion-mediated and does not require *aci*-nitro as key processor, therefore exhibits a higher quantum efficiency, faster release kinetics and less toxic photoproducts in contrast to *o*-NB mediated photolysis.

Attracted by these features, here three more photocages, DPAdCage, DAPdeCage and XDAPdeCage, are synthesized and characterized. DPAdCage is the first successfully characterized cage among the three and uses BPG as Zn^{2+} chelator (Fig 6.1 upper left, lower left). DAPdeCage and XDAPdeCage uses PDA as Zn^{2+} chelator (Fig 6.1 upper right, lower middle and right). Both BPG and PDA are highly chelating, tetradentate ligands that form 1:1 complexes with Zn^{2+} in aqueous solution^[55]. Structure characterization of the

[BPG-Zn(H₂O)₂]⁺ complex reveals Zn²⁺ adopts a distorted octahedral coordination where the BPG ligand donates three nitrogen atoms and one carboxylate oxygen atom, with the rest two coordination sites occupied by two water molecules^[58]. In a recent work done by an undergraduate in our group, the crystal structure of [Zn-DPAdeCage-Cl] was obtained from a mixture of DPAdeCage, ZnCl₂, pyridine and methanol, revealing a distorted trigonal bipyramid coordination geometry for the caged Zn²⁺ complex. Compared to NTAdCage, the introduction of pyridyl groups to DPAdeCage, DAPdeCage, and XDAPdeCage greatly improves the selectivity for Zn²⁺ over other competing metal ions such as Ca²⁺ and Mg²⁺. Moreover, both DAPdeCage and XDAPdeCage are membrane-permeable when complexed with Zn²⁺, therefore are much easier to be delivered into the cells. At physiological pH, DPAdeCage, DAPdeCage and XDAPdeCage have close K_d values and bind Zn²⁺ at a moderate pM level. The affinity is not as high as ZinClev-2 but close to ZinClev-1 and higher than *Cast*.

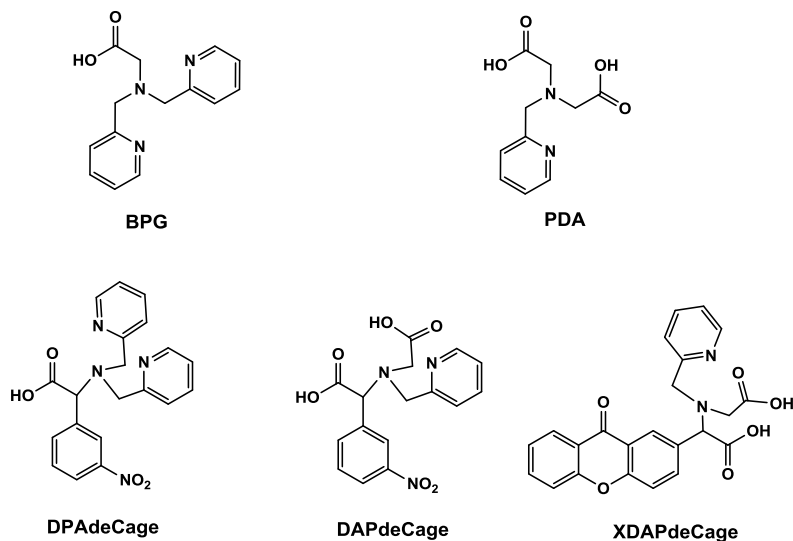


Fig 6.1 Structures of Zn²⁺ chelators and the corresponding Zn²⁺ cages developed.

The light-triggered Zn²⁺ uncaging from these photocages revealed a high efficient release kinetic. DPAdeCage and DAPdeCage are *m*-nitrobenzyl derivatives and have a quantum yield of 39% and 54% when Zn²⁺ is absent. When complexed with Zn²⁺, the quantum yields are 7.1%

and 5.9% respectively. The decreased quantum yield of Zn^{2+} -Cage complex is presumably due to the metal coordination which partially inhibits the imine formation. Even though, the quantum yields of $[\text{Zn}(\text{DPAdCage})]^+$ and $\text{Zn}(\text{DAPdeCage})$ are still significantly higher than the previously reported *Cast* and *Cleav* families. XDAPdeCage is derived from xanthone acetic acid and has a red shifted absorbance compared to benzyl derivatives. Photolysis of apo-XDAPdeCage and $\text{Zn}(\text{XDAPdeCage})$ lead to close quantum yield values: 17% for the apo and 13% for the Zn^{2+} . Further related investigation such as laser flash photolysis may assist a fully understanding of the metal-influenced radical reaction mechanism.

As a summary of the work, three new generations of photocages with moderate Zn^{2+} binding affinity have been developed. Compared with their predecessors, they use an alternative strategy based on the photo-induced decarboxylation and perform more efficient photolysis with less toxic photoproduct generated. Among the three, DAPdeCage and XDAPdeCage can form neutral-charged complex with Zn^{2+} and be delivered into the cells. This is the first time a Zn^{2+} Cage is reported to be cell-permeable with no necessary of extra modification, and will greatly facilitate the intracellular Zn^{2+} studies. Further work will include but not be limited to uncover the detailed photolysis mechanisms and employing the cages in neurological studies.

References

- [1] Josko, Osredkar. "Copper and zinc, biological role and significance of copper/zinc imbalance." *Journal of Clinical Toxicology* (2011).
- [2] Calesnick, B., and A. M. Dinan. "Zinc deficiency and zinc toxicity." *American family physician* 37, no. 4 (1988): 267.
- [3] Maret, Wolfgang. "Zinc biochemistry: from a single zinc enzyme to a key element of life." *Advances in Nutrition: An International Review Journal* 4, no. 1 (2013): 82-91.
- [4] Wang, Chu, Robert Vernon, Oliver Lange, Michael Tyka, and David Baker. "Prediction of structures of zinc-binding proteins through explicit modeling of metal coordination geometry." *Protein science* 19, no. 3 (2010): 494-506.
- [5] Sensi, Stefano L., Lorella MT Canzoniero, Shan Ping Yu, Howard S. Ying, Jae-Young Koh, Geoffrey A. Kerchner, and Dennis W. Choi. "Measurement of intracellular free zinc in living cortical neurons: routes of entry." *The Journal of neuroscience* 17, no. 24 (1997): 9554-9564.
- [6] Maret, Wolfgang. "Metals on the move: zinc ions in cellular regulation and in the coordination dynamics of zinc proteins." *Biometals* 24, no. 3 (2011): 411-418.
- [7] Krężel, Artur, and Wolfgang Maret. "Zinc-buffering capacity of a eukaryotic cell at physiological pZn." *JBIC Journal of Biological Inorganic Chemistry* 11, no. 8 (2006): 1049-1062.
- [8] Maret, Wolfgang. "Analyzing free zinc (II) ion concentrations in cell biology with fluorescent chelating molecules." *Metallomics* (2015).
- [9] Colvin, Robert A., William R. Holmes, Charles P. Fontaine, and Wolfgang Maret. "Cytosolic zinc buffering and muffling: their role in intracellular zinc homeostasis." *Metallomics* 2, no. 5 (2010): 306-317.
- [10] Thomas, Roger C., Jonathan A. Coles, and Jochen W. Deitmer. "Homeostatic muffling." *Nature* 350, no. 6319 (1991): 564.
- [11] Yamasaki, Satoru, Kumiko Sakata-Sogawa, Aiko Hasegawa, Tomoyuki Suzuki, Koki Kabu, Emi Sato, Tomohiro Kurosaki et al. "Zinc is a novel intracellular second messenger." *The Journal of cell biology* 177, no. 4 (2007): 637-645.
- [12] Maret, Wolfgang. "Zinc biochemistry: from a single zinc enzyme to a key element of life." *Advances in Nutrition: An International Review Journal* 4, no. 1 (2013): 82-91.
- [13] Rink, Lothar, and Hajo Haase. "Zinc homeostasis and immunity." *Trends in immunology* 28, no. 1 (2007): 1-4.

- [14] Hirano, Toshio, Masaaki Murakami, Toshiyuki Fukada, Keigo Nishida, Satoru Yamasaki, and Tomoyuki Suzuki. "Roles of zinc and zinc signaling in immunity: zinc as an intracellular signaling molecule." *Advances in immunology* 97 (2008): 149-176.
- [15] Miao, Yi-Liang, Paula Stein, Wendy N. Jefferson, Elizabeth Padilla-Banks, and Carmen J. Williams. "Calcium influx-mediated signaling is required for complete mouse egg activation." *Proceedings of the National Academy of Sciences* 109, no. 11 (2012): 4169-4174.
- [16] Kinsey, William H. "Intersecting roles of protein tyrosine kinase and calcium signaling during fertilization." *Cell calcium* 53, no. 1 (2013): 32-40.
- [17] Powell, M. J., M. S. Davies, and D. Francis. "THE INFLUENCE OF ZINC ON THE CELL CYCLE IN THE ROOT MERISTEM OF A ZINC-TOLERANT AND A NON-TOLERANT CULTIVAR OF FESTUCA RUBRA L." *New phytologist* 102, no. 3 (1986): 419-428.
- [18] POWELL, MJ, MS DAVIES, and D. FRANCIS. "Effects of zinc on cell, nuclear and nucleolar size, and on RNA and protein content in the root meristem of a zinc-tolerant and a non-tolerant cultivar of Festuca rubra L." *New phytologist* 104, no. 4 (1986): 671-679.
- [19] Kim, Alison M., Miranda L. Bernhardt, Betty Y. Kong, Richard W. Ahn, Stefan Vogt, Teresa K. Woodruff, and Thomas V. O'Halloran. "Zinc sparks are triggered by fertilization and facilitate cell cycle resumption in mammalian eggs." *ACS chemical biology* 6, no. 7 (2011): 716-723.
- [20] Que, Emily L., Reiner Bleher, Francesca E. Duncan, Betty Y. Kong, Sophie C. Gleber, Stefan Vogt, Si Chen et al. "Quantitative mapping of zinc fluxes in the mammalian egg reveals the origin of fertilization-induced zinc sparks." *Nature Chemistry* 7, no. 2 (2015): 130-139.
- [21] Kong, B. Y., F. E. Duncan, E. L. Que, A. M. Kim, T. V. O'Halloran, and T. K. Woodruff. "Maternally-derived zinc transporters ZIP6 and ZIP10 drive the mammalian oocyte-to-egg transition." *Molecular human reproduction* 20, no. 11 (2014): 1077-1089.
- [22] Lisle, Risa Stacey, Kate Anthony, M. A. Randall, and F. J. Diaz. "Oocyte–cumulus cell interactions regulate free intracellular zinc in mouse oocytes." *Reproduction* 145, no. 4 (2013): 381-390.
- [23] Bernhardt, Miranda L., Betty Y. Kong, Alison M. Kim, Thomas V. O'Halloran, and Teresa K. Woodruff. "A zinc-dependent mechanism regulates meiotic progression in mammalian oocytes." *Biology of reproduction* 86, no. 4 (2012): 114.
- [24] Shoji, Shisako, Yutaka Muto, Mariko Ikeda, Fahu He, Kengo Tsuda, Noboru Ohsawa, Ryogo Akasaka et al. "The zinc-binding region (ZBR) fragment of Emi2 can inhibit APC/C by targeting its association with the coactivator Cdc20 and UBE2C-mediated ubiquitylation." *FEBS open bio* 4 (2014): 689-703.

- [25] Kim, Alison M., Stefan Vogt, Thomas V. O'Halloran, and Teresa K. Woodruff. "Zinc availability regulates exit from meiosis in maturing mammalian oocytes." *Nature chemical biology* 6, no. 9 (2010): 674-681.
- [26] Li, Min, and Pumin Zhang. "The function of APC/CCdh1 in cell cycle and beyond." *Cell division* 4, no. 1 (2009): 2.
- [27] Kaplan, Jack H., Bliss Forbush III, and Joseph F. Hoffman. "Rapid photolytic release of adenosine 5'-triphosphate from a protected analog: utilization by the sodium: potassium pump of human red blood cell ghosts." *Biochemistry* 17.10 (1978): 1929-1935.
- [28] Milburn, Tracy, et al. "Synthesis, photochemistry, and biological activity of a caged photolabile acetylcholine receptor ligand." *Biochemistry* 28.1 (1989): 49-55.
- [29] Curley, Kieran, and David S. Lawrence. "Light-activated proteins." *Current opinion in chemical biology* 3.1 (1999): 84-88.
- [30] Chaulk, Steven G., and Andrew M. MacMillan. "Caged RNA: photo-control of a ribozyme reaction." *Nucleic acids research* 26.13 (1998): 3173-3178.
- [31] Gurney, Alison M. "Flash photolysis of caged compounds." *Microelectrode Techniques. The Plymouth Workshop Handbook*. The Company of Biologists, 1994.
- [32] Tsien, Roger Y., and ROBERT S. ZUCKER. "Control of cytoplasmic calcium with photolabile tetracarboxylate 2-nitrobenzhydrol chelators." *Biophysical journal* 50.5 (1986): 843.
- [33] Adams, S. R., et al. "Biologically useful chelators that release Ca²⁺ upon illumination." *Journal of the American Chemical Society* 110.10 (1988): 3212-3220.
- [34] Gyorko, Sandor, and Michael Fill. "Ryanodine receptor adaptation: control mechanism of Ca (2+)-induced Ca²⁺ release in heart." *Science* 260.5109 (1993): 807-809.
- [35] Ellis-Davies, G. C., Jack H. Kaplan, and Robert J. Barsotti. "Laser photolysis of caged calcium: rates of calcium release by nitrophenyl-EGTA and DM-nitrophen." *Biophysical journal* 70.2 (1996): 1006.
- [36] DelPrincipe, Franco, Marcel Egger, and Ernst Niggli. "Calcium signalling in cardiac muscle: refractoriness revealed by coherent activation." *Nature Cell Biology* 1.6 (1999): 323-329.
- [37] Ciesiński, Katie L., Kathryn L. Haas, Marina G. Dickens, Yohannes T. Tesema, and Katherine J. Franz. "A photolabile ligand for light-activated release of caged copper." *Journal of the American Chemical Society* 130, no. 37 (2008): 12246-12247.
- [38] Ciesiński, Katie L., Kathryn L. Haas, and Katherine J. Franz. "Development of next-generation photolabile copper cages with improved copper binding properties." *Dalton Transactions* 39.40 (2010): 9538-9546.

- [39] Gwizdala, Celina, and Shawn C. Burdette. "Following the Ca 2+ roadmap to photocaged complexes for Zn 2+ and beyond." *Current opinion in chemical biology* 17.2 (2013): 137-142.
- [40] Kennedy, Daniel P., Christopher D. Incarvito, and Shawn C. Burdette. "FerriCast: a macrocyclic photocage for Fe3+." *Inorganic chemistry* 49.3 (2010): 916-923.
- [41] Barbeau, K., E. L. Rue, K. W. Bruland, and A. Butler. "Photochemical cycling of iron in the surface ocean mediated by microbial iron (III)-binding ligands." *Nature* 413, no. 6854 (2001): 409-413.
- [42] Kennedy, Daniel P., Celina Gwizdala, and Shawn C. Burdette. "Methods for preparing metal ion photocages: application to the synthesis of crown-cast." *Organic letters* 11.12 (2009): 2587-2590.
- [43] Gwizdala, Celina, Daniel P. Kennedy, and Shawn C. Burdette. "ZinCast-1: a photochemically active chelator for Zn 2+." *Chemical Communications* 45 (2009): 6967-6969.
- [44] Bandara, HM Dhammika, Daniel P. Kennedy, Elif Akin, Christopher D. Incarvito, and Shawn C. Burdette. "Photoinduced release of Zn2+ with ZinCleav-1: a nitrobenzyl-based caged complex." *Inorganic chemistry* 48, no. 17 (2009): 8445-8455.
- [45] Gwizdala, Celina, Charlene V. Singh, Tracey R. Friss, John C. MacDonald, and Shawn C. Burdette. "Quantifying factors that influence metal ion release in photocaged complexes using ZinCast derivatives." *Dalton Transactions* 41, no. 26 (2012): 8162-8174.
- [46] Bandara, H. M., Timothy P. Walsh, and Shawn C. Burdette. "A Second - Generation Photocage for Zn2+ Inspired by TPEN: Characterization and Insight into the Uncaging Quantum Yields of ZinCleav Chelators." *Chemistry—A European Journal* 17.14 (2011): 3932-3941.
- [47] Basa, Prem N., Sagar Antala, Robert E. Dempski, and Shawn C. Burdette. "A Zinc (II) Photocage Based on a Decarboxylation Metal Ion Release Mechanism for Investigating Homeostasis and Biological Signaling." *Angewandte Chemie* 127, no. 44 (2015): 13219-13223.
- [48] Margerum, J. David, and Cunegunda T. Petrusis. "Photodecarboxylation of nitrophenylacetate ions." *Journal of the American Chemical Society* 91.10 (1969): 2467-2472.
- [49] Borsarelli, Claudio D., Silvia E. Braslavsky, Salvatore Sortino, Giancarlo Marconi, and Sandra Monti. "Photodecarboxylation of Ketoprofen in Aqueous Solution. A Time - resolved Laser - induced Optoacoustic Study." *Photochemistry and photobiology* 72, no. 2 (2000): 163-171.

- [50] Burns, Misty - Dawn, and Matthew Lukeman. "Efficient Photodecarboxylation of Trifluoromethyl - substituted Phenylacetic and Mandelic Acids." *Photochemistry and photobiology* 86, no. 4 (2010): 821-826.
- [51] Ding, Lina, Xuebo Chen, and Wei-Hai Fang. "Ultrafast asynchronous concerted excited-state intramolecular proton transfer and photodecarboxylation of o-acetylphenylacetic acid explored by combined CASPT2 and CASSCF studies." *Organic letters* 11, no. 7 (2009): 1495-1498.
- [52] Bowers, P. R., K. A. McLauchlan, and R. C. Sealy. "Photodecarboxylation of carboxylic acids sensitized by triplet benzophenone and duroquinone. A flash photolysis electron spin resonance and chemically induced dynamic nuclear polarization nuclear magnetic resonance investigation." *Journal of the Chemical Society, Perkin Transactions 2* 8 (1976): 915-921.
- [53] Blake, Jessie A., Eric Gagnon, Matthew Lukeman, and J. C. Scaiano. "Photodecarboxylation of xanthone acetic acids: CC bond heterolysis from the singlet excited state." *Organic letters* 8, no. 6 (2006): 1057-1060.
- [54] Okada, Keiji, Kazushige Okamoto, and Masaji Oda. "A new and practical method of decarboxylation: Photosensitized decarboxylation of N-acyloxyphthalimides via electron-transfer mechanism." *Journal of the American Chemical Society* 110, no. 26 (1988): 8736-8738.
- [55] Chiu, Yu-Hung, and James W. Canary. "Stability and acidity constants for ternary ligand-zinc-hydroxo complexes of tetradentate tripodal ligands." *Inorganic chemistry* 42, no. 17 (2003): 5107-5116.
- [56] Tanaka, Motoharu, Shigenobu Funahashi, and Kumiko Shirai. "Kinetics of the ligand substitution reaction of the zinc (II)-4-(2-pyridylazo) resorcinol complex with (ethylene glycol) bis (2-aminoethyl ether)-N, N, N', N'-tetraacetic acid." *Inorganic Chemistry* 7, no. 3 (1968): 573-578.
- [57] Xu, Zhaochao, Kyung-Hwa Baek, Ha Na Kim, Jingnan Cui, Xuhong Qian, David R. Spring, Injae Shin, and Juyoung Yoon. "Zn²⁺-triggered amide tautomerization produces a highly Zn²⁺-selective, cell-permeable, and ratiometric fluorescent sensor." *Journal of the American Chemical Society* 132, no. 2 (2009): 601-610.
- [58] Ibrahim, Mohamed M. "Synthesis and spectroscopic characterization of zinc (II) and copper (II) complexes of N, N-bis (2-picolyl) glycine as structural phosphotriesterase models: The catalyzed detoxification of paraoxon." *Journal of Molecular Structure* 990, no. 1 (2011): 227-236.
- [59] Gruenwedel, Dieter W. "Multidentate coordination compounds. Chelating properties of aliphatic amines containing. alpha.-pyridyl residues and other aromatic ring systems as donor groups." *Inorganic Chemistry* 7, no. 3 (1968): 495-501.

- [60] Alderighi, Lucia, Peter Gans, Andrea Ienco, Daniel Peters, Antonio Sabatini, and Alberto Vacca. "Hyperquad simulation and speciation (HySS): a utility program for the investigation of equilibria involving soluble and partially soluble species." *Coordination Chemistry Reviews* 184, no. 1 (1999): 311-318.
- [61] Maret, Wolfgang. "Zinc biochemistry: from a single zinc enzyme to a key element of life." *Advances in Nutrition: An International Review Journal* 4, no. 1 (2013): 82-91.
- [62] Kim, Alison M., Miranda L. Bernhardt, Betty Y. Kong, Richard W. Ahn, Stefan Vogt, Teresa K. Woodruff, and Thomas V. O'Halloran. "Zinc sparks are triggered by fertilization and facilitate cell cycle resumption in mammalian eggs." *ACS chemical biology* 6, no. 7 (2011): 716-723.
- [63] Que, Emily L., Reiner Bleher, Francesca E. Duncan, Betty Y. Kong, Sophie C. Gleber, Stefan Vogt, Si Chen et al. "Quantitative mapping of zinc fluxes in the mammalian egg reveals the origin of fertilization-induced zinc sparks." *Nature chemistry* 7, no. 2 (2015): 130-139.
- [64] Lacoste, R. G., G. V. Christoffers, and A. E. Martell. "New Multidentate Ligands. II. Amino Acids Containing α -Pyridyl Groups 1, 2." *Journal of the American Chemical Society* 87, no. 11 (1965): 2385-2388.
- [65] Blake, Jessie A., Matthew Lukeman, and Juan C. Scaiano. "Photolabile protecting groups based on the singlet state photodecarboxylation of xanthone acetic acid." *Journal of the American Chemical Society* 131, no. 11 (2009): 4127-4135.
- [66] Blake, Jessie A., Eric Gagnon, Matthew Lukeman, and J. C. Scaiano. "Photodecarboxylation of xanthone acetic acids: CC bond heterolysis from the singlet excited state." *Organic letters* 8, no. 6 (2006): 1057-1060.
- [67] Blake, Jessie A., Matthew Lukeman, and Juan C. Scaiano. "Photolabile protecting groups based on the singlet state photodecarboxylation of xanthone acetic acid." *Journal of the American Chemical Society* 131, no. 11 (2009): 4127-4135.
- [68] Fukada, Toshiyuki, and Taiho Kambe, eds. *Zinc Signals in Cellular Functions and Disorders*. Springer, 2014.